UNCLASSIFIED

AD NUMBER
ADB016324
LIMITATION CHANGES
TO: **Approved for public release; distribution is unlimited.**
FROM: **Distribution authorized to U.S. Gov't. agencies only; Test and Evaluation; SEP 1976. Other requests shall be referred to Air Force Armament Laboratory, Eglin AFB, FL 32542.**
AUTHORITY
USADTC ltr, 10 Apr 1980

THIS PAGE IS UNCLASSIFIED

AFATL-TR-76-104

CHARACTERIZATION OF THE SEISMIC MEDIUM USING NONLINEAR IDENTIFICATION TECHNIQUES

MINES BRANCH
MUNITIONS DIVISION

SEPTEMBER 1976

FINAL REPORT: MARCH 1976 - AUGUST 1976

Distribution limited to U. S. Government agencies only; this report documents test and evaluation; distribution limitation applied September 1976. Other requests for this document must be referred to the Air Force Armament Laboratory (DLJM), Eglin Air Force Base, Florida 32542.

AIR FORCE ARMAMENT LABORATORY
AIR FORCE SYSTEMS COMMAND • UNITED STATES AIR FORCE
EGLIN AIR FORCE BASE, FLORIDA

UNCLASSIFIED

SECURITY CLASSIFICATION OF THIS PAGE (When Data Entered)

REPORT DOCUMENTATION PAGE

READ INSTRUCTIONS BEFORE COMPLETING FORM

14

1. REPORT NUMBER: AFATL-TR-76-104

2. GOVT ACCESSION NO.

3. RECIPIENT'S CATALOG NUMBER

9

4. TITLE (and Subtitle)

6

CHARACTERIZATION OF THE SEISMIC MEDIUM USING NON-LINEAR IDENTIFICATION TECHNIQUES.

5. TYPE OF REPORT & PERIOD COVERED: Final Report. March 1976 — August 1976,

6. PERFORMING ORG. REPORT NUMBER

7. AUTHOR(s)

10

Raymond B. Walker,
James G. Constantine
Michael E. Warren

8. CONTRACT OR GRANT NUMBER(s)

9. PERFORMING ORGANIZATION NAME AND ADDRESS

Mines Branch, Munitions Division
Air Force Armament Laboratory
Armament Development and Test Center
Eglin Air Force Base, Florida 32542

10. PROGRAM ELEMENT, PROJECT, TASK AREA & WORK UNIT NUMBERS

Project No. 2510
Task No. 02
Work Unit No. ~~015~~

62602F

11. CONTROLLING OFFICE NAME AND ADDRESS

Air Force Armament Laboratory
Armament Development and Test Center
Eglin Air Force Base, Florida 32542

11

12. REPORT DATE: September 1976

13. NUMBER OF PAGES: 52

14. MONITORING AGENCY NAME & ADDRESS (if different from Controlling Office)

12 52p.

15. SECURITY CLASS. (of this report): UNCLASSIFIED

15a. DECLASSIFICATION/DOWNGRADING SCHEDULE

16. DISTRIBUTION STATEMENT (of this Report)

Distribution limited to U.S. Government agencies only; this report documents test and evaluation; distribution limitation applied September 1976. Other requests for this document must be referred to the Air Force Armament Laboratory (DLJM), Eglin Air Force Base, Florida 32542.

17. DISTRIBUTION STATEMENT (of the abstract entered in Block 20, if different from Report)

16 2510 17 02

18. SUPPLEMENTARY NOTES

Available in DDC

19. KEY WORDS (Continue on reverse side if necessary and identify by block number)

Nonlinear Identification Techniques
White Noise Signal
Near Field Seismic Propagation Medium

20. ABSTRACT (Continue on reverse side if necessary and identify by block number)

The near field seismic propagation medium was characterized using Wiener's nonlinear identification techniques. The system stimulus was a white noise signal generated by an audio system and measured by a microphone placed directly in front of the speaker. The output signal was measured by a geophone placed at predetermined intervals down range from the speaker. The first and second order Wiener kernels of the system were determined, and it was conclusively shown that the system exhibits nonlinearities. The calculated kernels were then used

NEXT page

LB

DD FORM 1 JAN 73 1473 EDITION OF 1 NOV 65 IS OBSOLETE

UNCLASSIFIED

SECURITY CLASSIFICATION OF THIS PAGE (When Data Entered)

400 936

(Item 20 concluded) to predict an output for a given input. Comparison of the predicted output with that of the measured output indicates that the physical system can be more accurately characterized by the first and second order Wiener kernels than by use of linear models.

PREFACE

This report documents the results of a study conducted by Lt Colonel Raymond B. Walker of the Mines Branch of the Munitions Division. The study was conducted during the period from March 1976 to August 1976.

This technical report has been reviewed and is approved for publication.

FOR THE COMMANDER:

WILLIAM F. BROCKMAN, Colonel, USAF
Chief, Munitions Division

(The reverse of this page is blank.)

TABLE OF CONTENTS

LIST OF FIGURES

LIST OF FIGURES (Concluded)

LIST OF TABLES

SECTION I

INTRODUCTION

Recent advances in sensor technology have led to increased interest in the detection and classification of various objects through use of their emitted energy. Two forms of emitted energy which appear to be very promising for classifying a wide variety of objects are the passively generated seismic and acoustic signals.

Many attempts have been made to detect and classify objects by processing the signals detected by geophones or microphones. These attempts have had limited success because of a lack of understanding of the signal source and of the properties of the propagation medium--in these cases, the ground and atomsphere.

Many studies of pure seismic waves, such as those generated by underground explosives or earthquakes, have been conducted and good seismic models have been developed (White, 1965). In the near field, however, both seismic and acoustic energy can couple into the ground and be detected by the geophone.

There is an interaction between the acoustic signal and the seismic medium throughout the length of the propagation channel. The signal sources of interest generate both seismic energy, which is coupled directly into the ground and propagated through the ground to the geophone, and acoustic energy which is coupled directly into the ground and also transmitted through the atmosphere. Throughout the propagation channel there is an interaction between the acoustic signal and the seismic media along the interface between the ground and the atmosphere. Part of the acoustic energy is absorbed, and part is reflected. This interface interaction produces a nonlinear effect, which is evidenced by the appearance of harmonics in the output when a clear tone is used as a stimulus.

In this research, the Wiener theory of nonlinear system identification was used to characterize the propagation channel associated with near field seismic/acoustic propagation and coupling. This theory requires the measurement of the system response to an input of zero mean white Gaussian noise. The system, S, in this case is the ground and atmosphere between the signal source and a geophone located distance, r, from the source. The input to the system is an audio system, consisting of an amplifier and speaker, driven by a noise generator.

The basic mathematics for nonlinear identification theory was developed by Norbert Wiener (1958). Lee and Schetzen (1965) further improved the Wiener theory by developing a cross-correlation technique which made it adaptable to digital computers. French and Butz (1973) showed how the computing time could be reduced through the use of fast Fourier transforms.

The potential to obtain a wide range of system response characteristics from a single experiment using nonlinear identification techniques has been recognized by researchers in the field. Several studies have centered on the identification of biological systems of animals. Marmarelis (1972) used the cross-correlation techniques of Lee and Schetzen to yield a functional description of the horizontal, bipolar, and ganglion cells in the vertebrate retina of the catfish. Marmarelis and McCann (1973) used the cross-correlation techniques to characterize the visual system of flies. McCann (1974) continued to make use of the nonlinear identification theory to study the photoreceptors and optokinetic flight response of flies. Current research is underway at the University of Florida by Brownell and Warren (1976) to study the response of the inner ear of cats to white noise stimulus.

The Wiener theory is a generalized method of analyzing a nonlinear system. Although previous use of the theory has been almost exclusively in the analysis of biological systems, the theory is applicable to most systems that are time-invariant and have finite memory. Therefore, it covers a very wide range of physical systems.

Section II of this report, the background theory of nonlinear identification is briefly reviewed. Section III provides a description of the experimental equipment and procedure. Data analysis and results are discussed in Section IV, with conclusions and recommendations for future research presented in Sections V and VI, respectively.

SECTION II

BACKGROUND THEORY

Wiener expressed the output of a nonlinear system in terms of an orthogonal set of G-functionals:

$$y(t) = \sum_{n=0}^{\infty} G_n\left[h_n, x(t)\right] \tag{1}$$

where the $\{h_n\}$ are the Wiener kernels of the system and the $\{G_n\}$ is a complete set of orthogonal functionals when the input, x(t), is a white Gaussian process. Each G_n is made up of multidimensional convolution integrals of degree n or less. The first three G-functionals are:

$$G_0\left[h_0, x(t)\right] = h_0$$

$$G_1\left[h_1, x(t)\right] = \int_{-\infty}^{\infty} h_1(\tau)x(t-\tau)d\tau$$

$$G_2\left[h_2, x(t)\right] = \int_{-\infty}^{\infty}\int_{-\infty}^{\infty} h_2(\tau_1,\tau_2)\,x\left(t-\tau_1\right)x\left(t-\tau_2\right)d\tau_1 d\tau_2 - A\int_{-\infty}^{\infty} h_2(\tau,\tau)d\tau \tag{2}$$

where $A\delta(t)$ is the autocorrelation function of the zero-mean white Gaussian process, x(t), and $\delta(t)$ is the unit impulse function. The nth degree G-functional is made of an nth order convolution:

$$\int_{-\infty}^{\infty}\cdots\int_{-\infty}^{\infty} h_n\left(\tau_1\ldots,\tau_n\right)x\left(t-\tau_1\right)\ldots x\left(t-\tau_n\right)d\tau_1\ldots d\tau_n$$

plus homogeneous functionals of lower order with kernels solely dependent upon h_n, derived in such a manner that G_n is orthogonal to all functionals of degree less than n.

In this formulation the identification problem is the determination of the Wiener kernels, h_n, of the system. The input and output of the system must be clearly defined, and the input must be a zero mean Gaussian white noise. Note that if the input is not white but may be represented as the response of a linear filter to white noise, there is a procedure discussed by Lee and Schetzen (1965) for whitening the input. With the input and output known, the orthogonality of the $\{G_n\}$ allows identification of the Wiener kernels.

Wiener originally expanded the kernels in terms of a set of Laguerre polynomials, although any complete orthogonal set would have served the same purpose. He then constructed a system (see Figure 1) whose response to a white Gaussian input was a G-functional with leading term containing a kernel consisting of a product of Laguerre polynomials. Then by correlating the response of this system with the response of the unknown system to the same input, the coefficients of the Laguerre expansion could be determined.

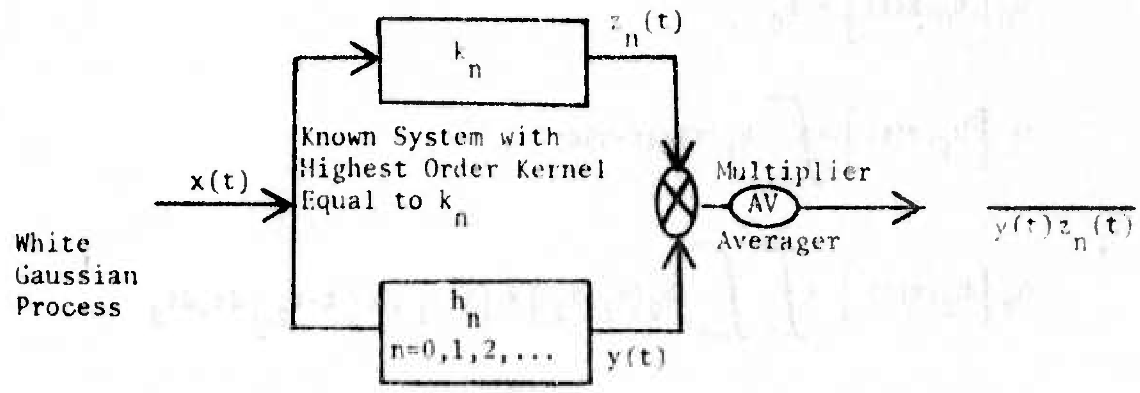

Figure 1. Wiener's Scheme for Measuring Kernels

The identification method proposed by Wiener allows the direct measurement of the Laguerre coefficients through synthesis by appropriate analog circuits. Practical considerations, however, require finite expansions which result in unavoidable truncation errors. These errors will be the minimum integral square errors associated with expansion of a function by a finite orthogonal set. The Wiener expansion and measurement scheme, therefore, approximates the kernels in a minimum integral square sense over the entire domain of the kernel.

While the Wiener method is more applicable to analog measurements, other methods have been devised which are more suitable for digital computation of the kernels. These are the cross-correlation method of Lee and Schetzen (1965) and the fast Fourier transform (FFT) method of French and Butz (1973).

The cross-correlation method of Lee and Schetzen allows the computation of the Wiener kernels without expansion in terms of an orthogonal set. This technique may be used to compute the kernels point-by-point in terms of simple time delays, σ_i. The analogous known system for this method is made up of parallel time delay filters (see Figure 2) for which the impulse response is $\delta(t-\sigma_i)$. The output from each filter is $x(t-\sigma_i)$.

The zero order kernel, $G_0[h_0,x(t)] = h_0$, is the average value of $y(t)$ for the input $x(t)$:

$$h_0 = \overline{y(t)} \tag{3}$$

where the bar is used to denote time average. Note that $x(t-\sigma_1)$ is a functional of the first order, that is

$$x(t-\sigma_1) = \int_{-\infty}^{\infty} \delta(\tau-\sigma_1)\, x(t-\tau)d\tau \tag{4}$$

Therefore, in the averaging of $y(t)x(t-\sigma_1)$, all averages involving G-functionals of order 2 and higher will disappear because of their orthogonal construction. Then

$$\overline{y(t)x(t-\sigma_1)} = \lim_{T\to\infty} \frac{1}{2T}\int_{-T}^{T} \{G_1[h_1,x(t)] + h_0\}\, x(t-\sigma_1)dt$$

$$= \lim_{T\to\infty} \frac{1}{2T}\int_{-T}^{T}\int_{-\infty}^{\infty} h_1(\tau)x(t-\tau)x(t-\sigma_1)\, d\tau dt + \lim_{T\to\infty} \frac{1}{2T}\int_{-T}^{T} h_0 x(t-\sigma_1)dt$$

$$= \int_{-\infty}^{\infty} h_1(\tau)A\delta(\tau-\sigma_1)\, d\tau$$

$$= Ah_1(\sigma_1) \tag{5}$$

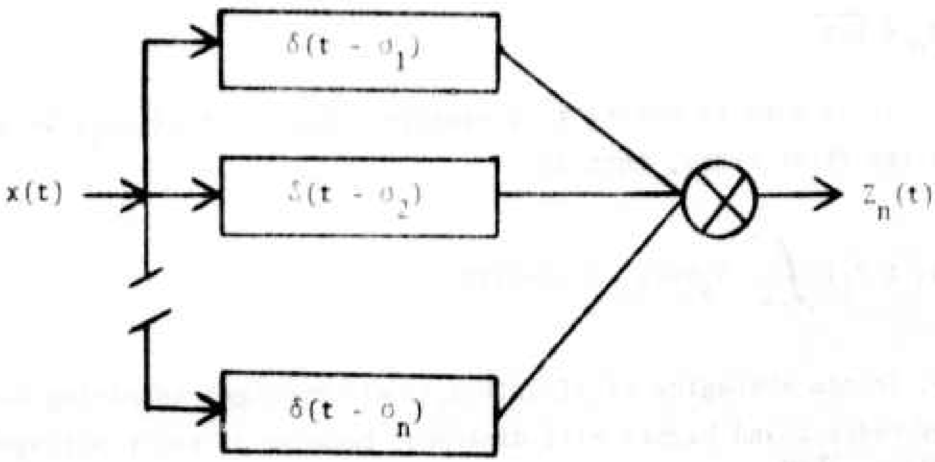

Figure 2. Known System for Cross-Correlation Measurements

Therefore,

$$h_1(\sigma_1) = \frac{1}{A}\overline{y(t)x(t-\sigma_1)} \tag{6}$$

The second order kernel is computed by the same process revealing:

$$h_2(\sigma_1,\sigma_2) = \frac{1}{2A^2}\overline{y(t)x(t-\sigma_1)x(t-\sigma_2)} - h_0\delta(\sigma_1-\sigma_2) \tag{7}$$

The second term in h_2 is an impulse at $\sigma_1 = \sigma_2$ which results from the averaging process of lower order terms. Since the lower order terms are known, they may be subtracted from $y(t)$ prior to the averaging process which eliminates the impulse. Then:

$$h_2(\sigma_1,\sigma_2) = \frac{1}{2A^2}\overline{[y(t)-h_0]x(t-\sigma_1)x(t-\sigma_2)} \tag{8}$$

for all σ_1, σ_2.

In general,

$$h_n(\sigma_1 \ldots \sigma_n) = \frac{1}{n!A^n}\overline{\left\{y(t) - \sum_{m=0}^{n-1} G_n[h_n, x(t)]\right\} x(t-\sigma_1) \ldots x(t-\sigma_n)} \tag{9}$$

In the FFT method of French and Butz (1973), the time functions $x(t)$, $y(t)$ and $h_n(\sigma_1 \ldots \sigma_n)$, for $n>0$, are expressed in their Fourier transform representation, respectively, $X(f)$, $Y(f)$, and $H_n(f_1, \ldots, f_n)$ where upper case letters are used to denote Fourier transforms. Also, complex exponential filters, with impulse response $e^{-j2\pi f_i t}$, are used instead of the time delay filters used in the cross-correlation method. The functional representation of the output $z_n(t)$ of the known system then becomes:

$$\begin{aligned} z_n(t) &= \int_{-\infty}^{\infty} \ldots \int_{-\infty}^{\infty} e^{-j(f_1\tau_1 + \ldots + f_n\tau_n)} x(t-\tau_1) \ldots x(t-\tau_n) d\tau_1 \ldots d\tau_n \\ &= X^*(f_1) \ldots X^*(f_n) e^{-j2\pi(f_1 + \ldots + f_n)t} \end{aligned} \tag{10}$$

where the asterisk denotes complex conjugate.

The zero order kernel is just $H(0) = Y(0) = \overline{y(t)} = h_0$, while the French and Butz expressions for the Fourier transform of the first and second order kernels are:

$$H_1(f) = \frac{1}{A} Y(f) X^*(f)$$

$$H_2\left(f_1, f_2\right) = \frac{1}{2A^2} Y\left(f_1 + f_2\right) X^*\left(f_1\right) X^*\left(f_2\right) - \frac{H_0}{2A} \delta\left(f_1 + f_2\right) \tag{11}$$

The Fourier transform of a white Gaussian process is again a stochastic process; hence, the kernels calculated by Equation (11) for a given sample input will represent only one sample of the respective kernels. To obtain the true kernels, an ensemble average must be performed. The requirement for ensemble averaging becomes apparent when consideration is given to the fact that the second order kernel must be zero for a linear system. The second order transfer function is a filter which passes that portion of the output at frequency $\left(f_1 + f_2\right)$ which is dependent on the input at frequencies f_1 and f_2. If the system is linear, there are no output values at frequency $\left(f_1 + f_2\right)$ except those which are caused by an input at frequency $\left(f_1 + f_2\right)$. Therefore, the second order kernel must be zero for a linear system. Without ensemble averaging, this is not the case.

The frequency domain kernels are therefore defined as

$$H_1(f) = \frac{1}{A} \langle Y(f) X^*(f) \rangle \tag{12}$$

and

$$H_2\left(f_1, f_2\right) = \frac{1}{2A^2} \langle Y\left(f_1 + f_2\right) X^*\left(f_1\right) X^*\left(f_2\right) \rangle \tag{13}$$

The discrete Fourier transform, $F(k\Delta f)$, used in this computation is

$$F(k\Delta f) = \frac{1}{N} \sum_{n=0}^{N-1} f(n\Delta t) e^{-j2\pi kn/N} \tag{14}$$

where N is the number of data samples at sampling interval Δt and $f(n\Delta t)$ is the sampled time function.

A is defined as the power spectral density (PSD) of the white noise input x(t). The theory assumes that the PSD of the input is constant. In practice, however, the actual input noise source exhibits a flat PSD over only a finite range of frequencies and even in this range, the PSD is not exactly constant. In this research the PSD of the source was computed by averaging the flat region of the sampled PSD from 50 to 1000 hertz and then ensemble averaging 40 data samples.

When the kernels and the input and output signals are expressed in their respective Fourier transform representation, the first three G-functionals from Equation (2) become

$$G_0[h_0, x(t)] = H_0$$

$$G_1[h_1, x(t)] = \int_{-\infty}^{\infty} H_1(f)X(f)e^{j2\pi ft}df$$

$$G_2[h_2, x(t)] = \int_{-\infty}^{\infty}\int_{-\infty}^{\infty} H_2\left(f_1, f_2\right)X\left(f_1\right)X\left(f_2\right)e^{j2\pi\left(f_1 + f_2\right)t}df_1df_2 - A\int_{-\infty}^{\infty} H_2(f, -f)df \tag{15}$$

SECTION III

EXPERIMENTAL ARRANGEMENT

The experimental arrangement for measuring input and output signals is depicted in Figure 3. The experiment consisted of playing broadband noise into a loudspeaker. The speaker output was used to excite the medium. The input signal was generated by a low frequency noise generator amplified by a Sansui 5000A 100-watt amplifier. Speaker output was measured by a microphone located directly in front of the speaker. System output measurements were taken by geophones located at intervals of 10, 20, 30, and 50 feet from the speaker. A geophone was located directly beneath the speaker to measure seismic energy transferred directly by the speaker enclosure. Microphone measurements were also taken concurrently with each output geophone for a related experiment involving the investigation of acoustic coupling properties. The signals were recorded on magnetic tape by an Ampex 2200 FM recorder. A Tektronix 434 Oscilloscope and a Nicolet 440A Mini Ubiquitous Spectrum Analyzer were used to monitor the signals during the recording process.

The noise generator was a General Radio Company 1381 Random Noise Generator with operating modes of 2 hertz to 50 kilohertz, 2 hertz to 20 kilohertz, or 2 hertz to 2 kilohertz. A Tektronics function generator provided an external filter which could be used to further decrease the noise bandwidth.

The speaker system was a Pioneer CS-99 system which contains a 12-inch woofer plus a 5-inch midrange and 2 horn tweeters. The speaker performed very poorly in the lower frequency region. Speaker response was relatively flat from 60 to 600 hertz, but speaker power decreased rapidly between 600 and 700 hertz due to crossover effects. The Pioneer speaker was replaced during the latter part of the test by a 15-inch Altec 416-8A speaker. The Altec speaker was capable of responding to tones as low as 30 hertz; however, a proper enclosure was not available for this speaker at the time of the experiment which caused poor quality data.

Table 1 provides a complete listing of equipment along with manufacturers' names and identifying numbers and the estimated or rated frequency response range.

Preliminary measurements of the system response to discrete tones of 30 to 2000 hertz were taken to determine the frequency response range of the system. System response above 700 hertz was nil. These measurements also provided information on system nonlinearity and for determination of sampling rate for the digital analysis. In changing from one tone value to the next, a frequency sweep was made to provide data for cross-correlation.

Noise samples were taken in the frequency ranges 2-2000 KHz, 2-1000 Hz,

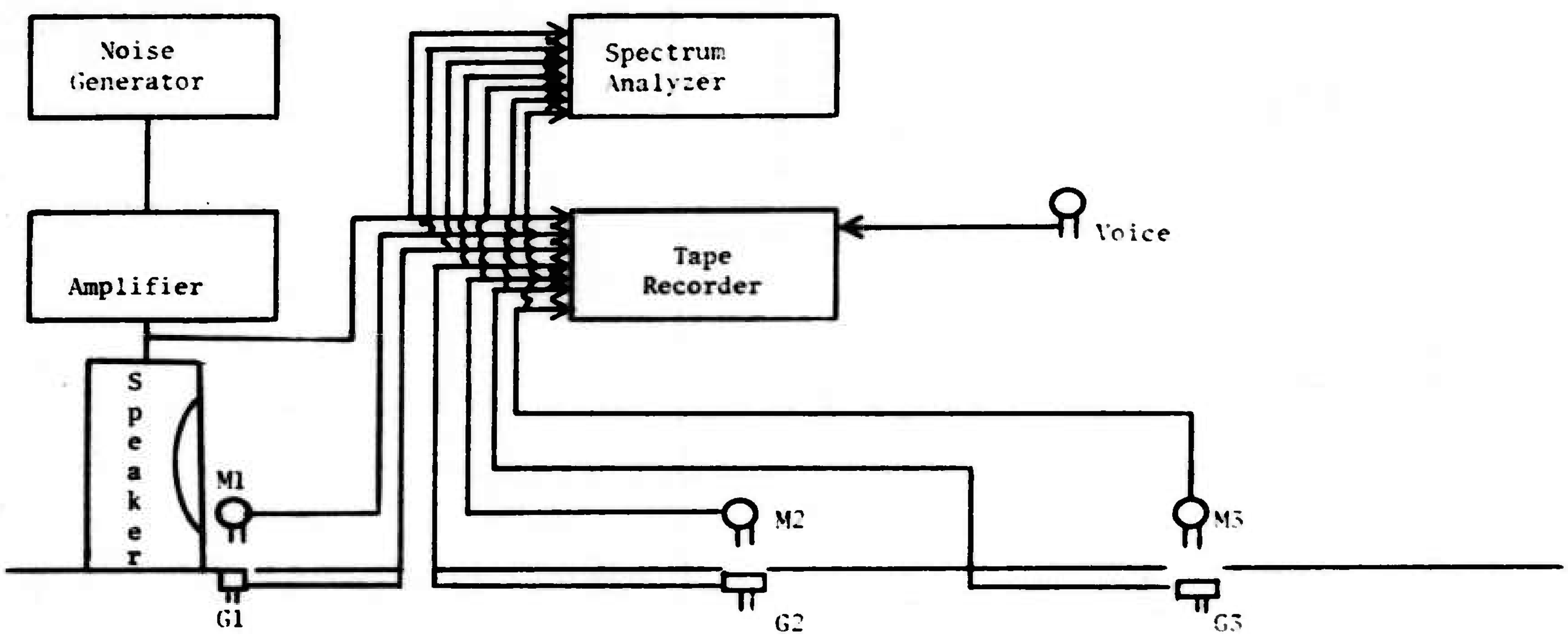

G1 Geophone 1

G2 Geophone 2

G3 Geophone 3

M1 Microphone 1

M2 Microphone 2

M3 Microphone 3

Figure 3. Experimental Arrangement

TABLE 1. LIST OF EQUIPMENT

ITEM	MANUFACTURER	MODEL NO. (TYPE)	FREQUENCY RESPONSE RANGE
Speaker	Pioneer	CS-99	60 Hz-600 Hz
Power Amplifier	Sansui	5000A	15 Hz-20 KHz
Noise Generator	General Radio Co.	1381	2 Hz-50 KHz
Microphone	General Radio Co.	Electret 1961-9601	5 Hz-15 KHz
Oscilloscope	Tektronix	434	
Spectrum Analyzer	Nicolet	440A Mini Ubiquitous	
Geophones	Geospace Corp.	Pat., 3119978 Vertical Axis	1 Hz-10 KHz
Recorder	Ampex	PR220 FM	0-40 KHz
Speaker	Altec	416-8A	30-1600 Hz
Function Generator	Tektronix	FG-502	

2-500 Hz, 2-300 Hz, 2-100 Hz, and 200-300 Hz. Other input signals included: impulses created by striking a metal plate with a hammer in the near vicinity of the input microphone and geophone; engine noise created by parking a 1/2-ton van with engine and/or muffler directly over the inputs; and vehicle signals created by making engine on and engine off passes at 5- and 10-MPH speeds by the inputs.

Signals from the following sensors were recorded during the experiment:

- The input from the noise generator (X).
- Microphone 1 (M1) collocated with the source.
- Geophone 1 (G1) collocated with the source at ground level and at 12 inches below ground level.
- Microphone 2 (M2) spaced alternately at 10 and 30 feet from the source.
- Geophone 2 (G2) spaced alternately at 10 and 30 feet from the source at ground level and also at 12 inches below ground level.
- Microphone 3 (M3) spaced alternately at 20 and 50 feet from the source.
- Geophone 3 (G3) spaced alternately at 20 and 50 feet from the source at ground level and also at 12 inches below ground level.

Recording arrangement on the 7-channel Ampex recorder was as follows:

CHANNEL	SIGNAL
1	M1
2	M2
3	G1
4	G2
5	M3
6	X
7	G3
Edge Track	Voice

This arrangement maintained the collocated microphone and geophone signals together on the same tape head for cross-correlation purposes.

Data were taken at two locations. Measurements were made at each site both with the speaker sitting upright on the ground facing the array and with the speaker lying face down on the ground. Array spacing, location, and speaker configuration for each experiment are shown in Table 2.

Site 1 was bordered to the west by concrete and to the north by an asphalt-covered roadway. House trailers were parked approximately 50 feet to the south of the array. The input sensors were located 10 feet from the concrete with the output sensors spaced to the east which was an open area. The soil at Site 1 was primarily red clay covered by grass. There was road construction in progress approximately 1 mile to the east which could be measured by the geophone.

Site 2 was primarily open area with a highway approximately 100 feet to the south. The soil at Site 2 was primarily sand sparsely covered by vegetation. The array was spaced south to north.

Table 2 shows the site, speaker configuration and distance from the source, and depth of G2 and G3 for each experiment performed. Each experiment consisted of the recording of impulses, clear tones, swept tones, random noise, and vehicle signatures.

TABLE 2. DETAILED DATA ON EXPERIMENTS

EXPERIMENT NUMBER	SITE	SPEAKER CONFIGURATION	G2 DISTANCE/DEPTH	G3 DISTANCE/DEPTH
1	1	Upright	10 ft/surface	20 ft/surface
2	1	Upright	10 ft/12 in	20 ft/12 in
3	1	Facing down	10 ft/12 in	20 ft/12 in
4	1	Upright	30 ft/12 in	50 ft/12 in
5	1	Facing down	30 ft/12 in	50 ft/12 in
6	1	Upright	30 ft/surface	50 ft/surface
7*	1	Upright	30 ft/8 in	30 ft/surface
8	2	Upright	10 ft/surface	20 ft/surface
9	2	Upright	30 ft/surface	50 ft/surface
10	2	Facing down	30 ft/surface	50 ft/surface
11	2	Upright	30 ft/12 in	50 ft/12 in
12*	2	Upright	30 ft/8 in	30 ft/surface

*G1 located at 30 feet from source, 16 inches deep.

The analog data was recorded on three 10-inch-diameter reels, designated Tapes 1, 2, and 3. Since all seven channels of the 1/2-inch-wide tape were used in the data collection, there was no room on the original tape for a time code. Therefore, dubs of the analog data were made on 1-inch-wide tape and the dubbed tapes were time-coded. A strip chart analysis was performed to associate each signal with a time code. Each signal was given a 5-digit designation. The first digit identifies the original data tape, the second and third digits identify the experiment number, and the fourth and fifth digits identify a particular signal in the experiment. Appendix A contains a listing of the signal numbers, the inclusive time code, and type signal.

SECTION IV

DATA ANALYSIS

The data analysis consisted of preliminary investigations in the laboratory and then calculation and evaluation of first and second order kernels.

PRELIMINARY ANALYSIS

Preliminary analyses of the data were performed in the laboratory to determine digitization rate, some idea of how many kernels should be computed, and system memory. Also the inputs M1 and G1 had to be evaluated for whiteness. The impulses and clear tone signals were examined with a spectrum analyzer and an X-Y plotter. Also the PSD of the various noise samples from each sensor and the vehicle signals were examined on the spectrum analyzer to determine bandwidth and relative energy content.

Analysis of the clear tone signals revealed that for frequencies higher than 700 hertz, the response of the geophone was at the level of ambient noise. It was therefore decided to digitize all signals at 2048 samples per second to allow the identification of all frequencies up to 1000 hertz. All signals were low-pass filtered at 1000 hertz to prevent aliasing.

Examination of the system response to clear tone inputs provides some insight into the order of nonlinearity of the system which, in turn, provides some guidance on how many kernels need be computed. A model that includes up to the nth order term can produce at most an nth order harmonic (Marmarelis, 1972).

Clear tone responses were analyzed by replaying the recorded tapes through a spectrum analyzer and plotting the results on an X-Y plotter, with a linear scale as shown in Figures 4 through 7. At 50 hertz, there is a second harmonic in the speaker output M1. This harmonic and several others show up in the geophone outputs. This indicates that the audio system as well as the seismic medium is nonlinear. At 100 and 200 hertz, the speaker harmonics have practically disappeared but the second harmonic in the geophones is still pronounced. At 300 hertz, the geophone harmonics are gone but a trace of a second harmonic has reappeared in the speaker. At 500 hertz all harmonics are gone. This indicates that the acoustic seismic interaction along the interface of the channels becomes less prevalent in the higher frequencies and could mean that the higher frequencies do not couple into the soil as well as the lower frequencies.

Figure 4 indicates that the nonlinearity of the total system is fourth order or higher. The total system includes the audio system and the seismic medium. It is suspected that the fourth harmonic seen in the geophone signals at 50 hertz is caused by the second harmonic from the speaker. Alsc

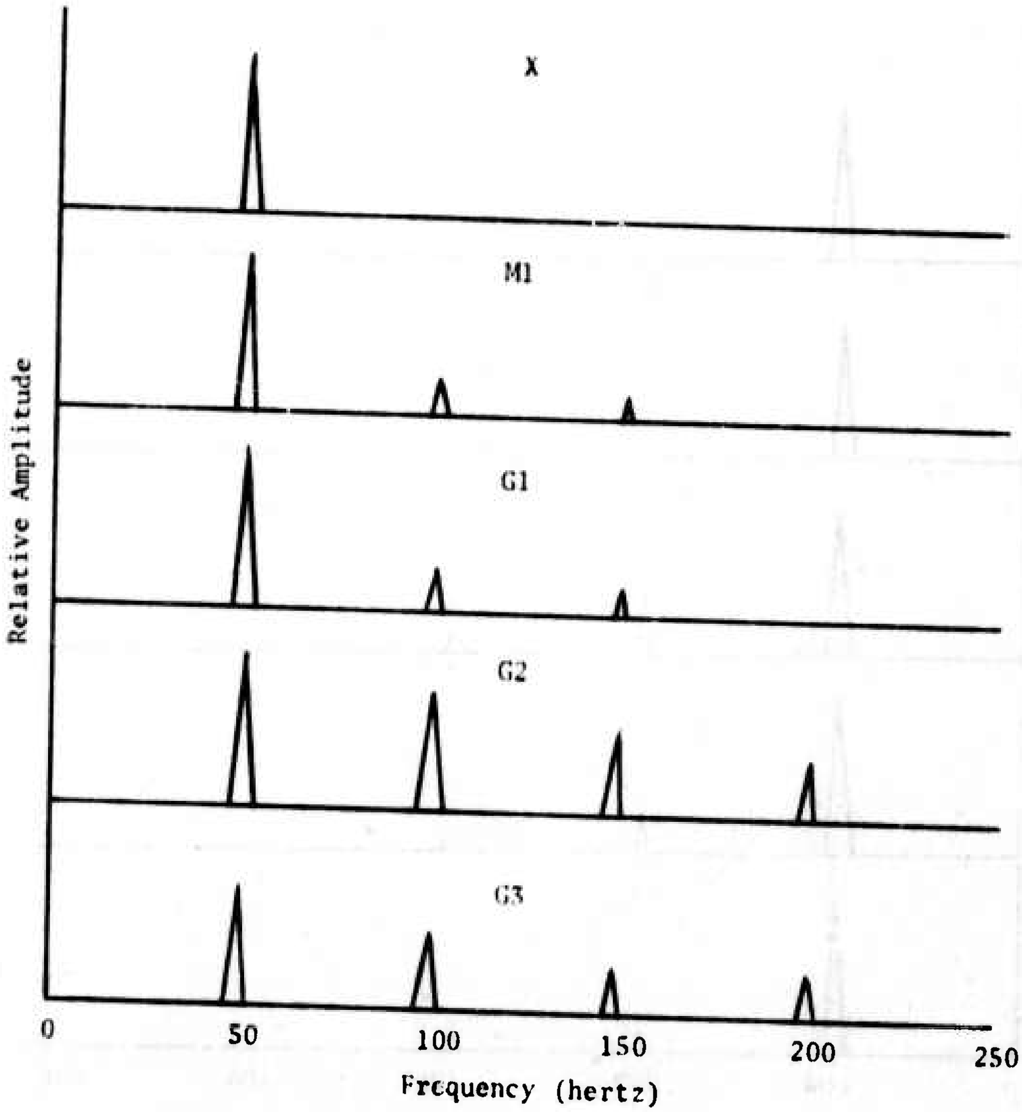

X Input Signal

M1 Signal at Microphone 1

G1 Signal at Geophone 1

G2 Signal at Geophone 2

G3 Signal at Geophone 3

Figure 4. System Harmonics at 50-Hertz Input

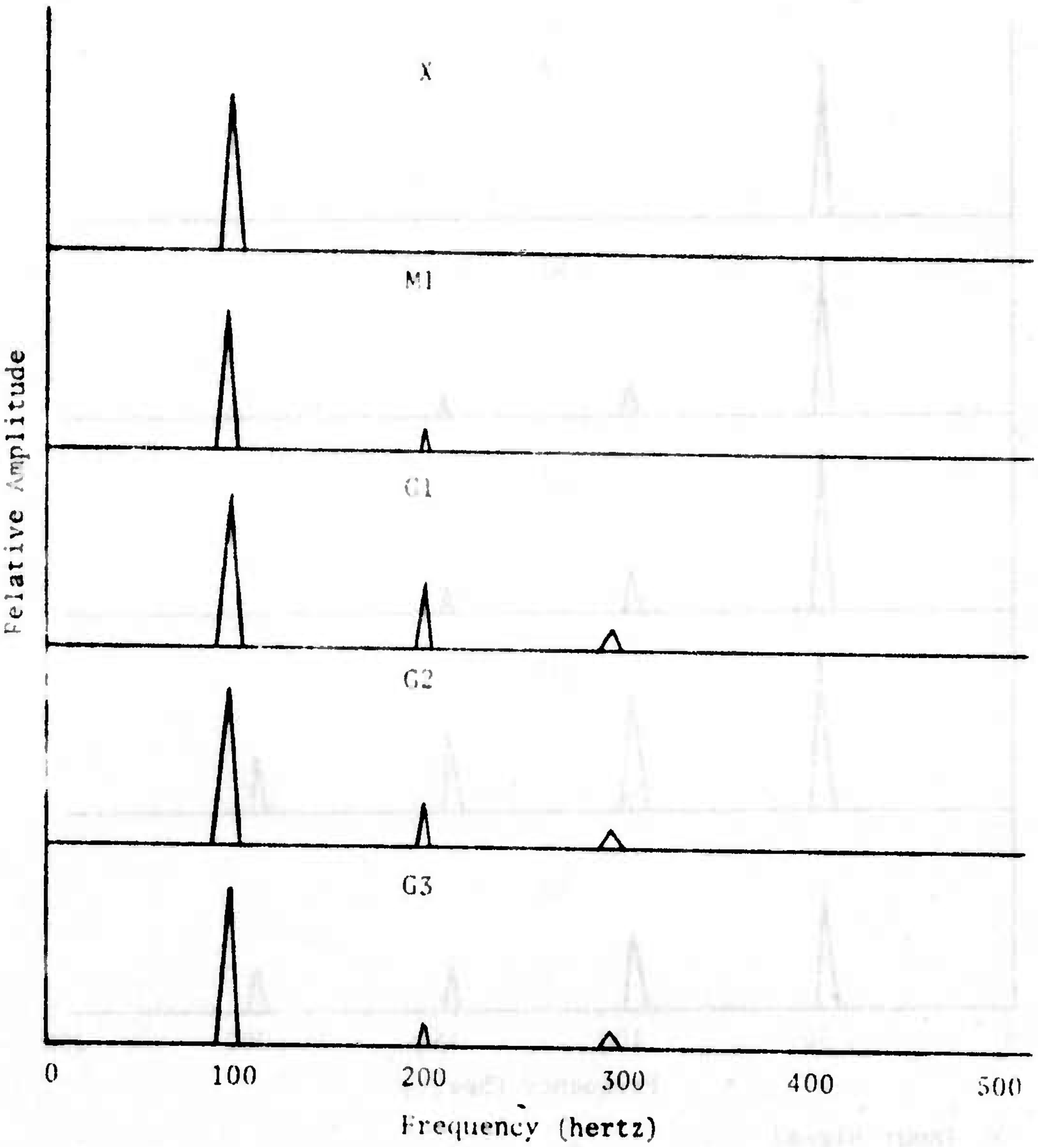

X Input Signal

M1 Signal at Microphone 1

G1 Signal at Geophone 1

G2 Signal at Geophone 2

G3 Signal at Geophone 3

Figure 5. System Harmonics at 100-Hertz Input

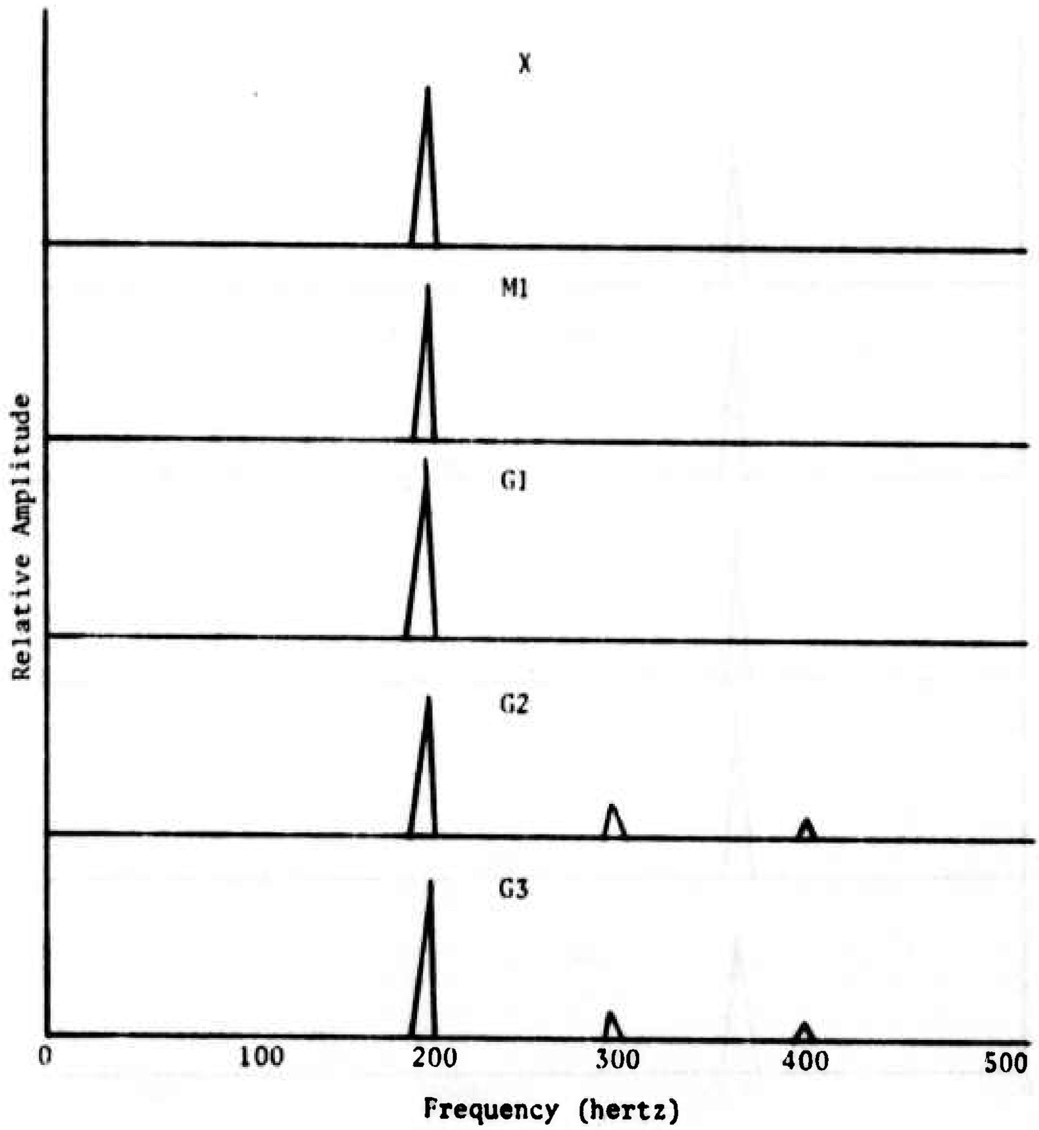

X Input Signal

M1 Signal at Microphone 1

G1 Signal at Geophone 1

G2 Signal at Geophone 2

G3 Signal at Geophone 3

Figure 6. System Harmonics at 200-Hertz Input

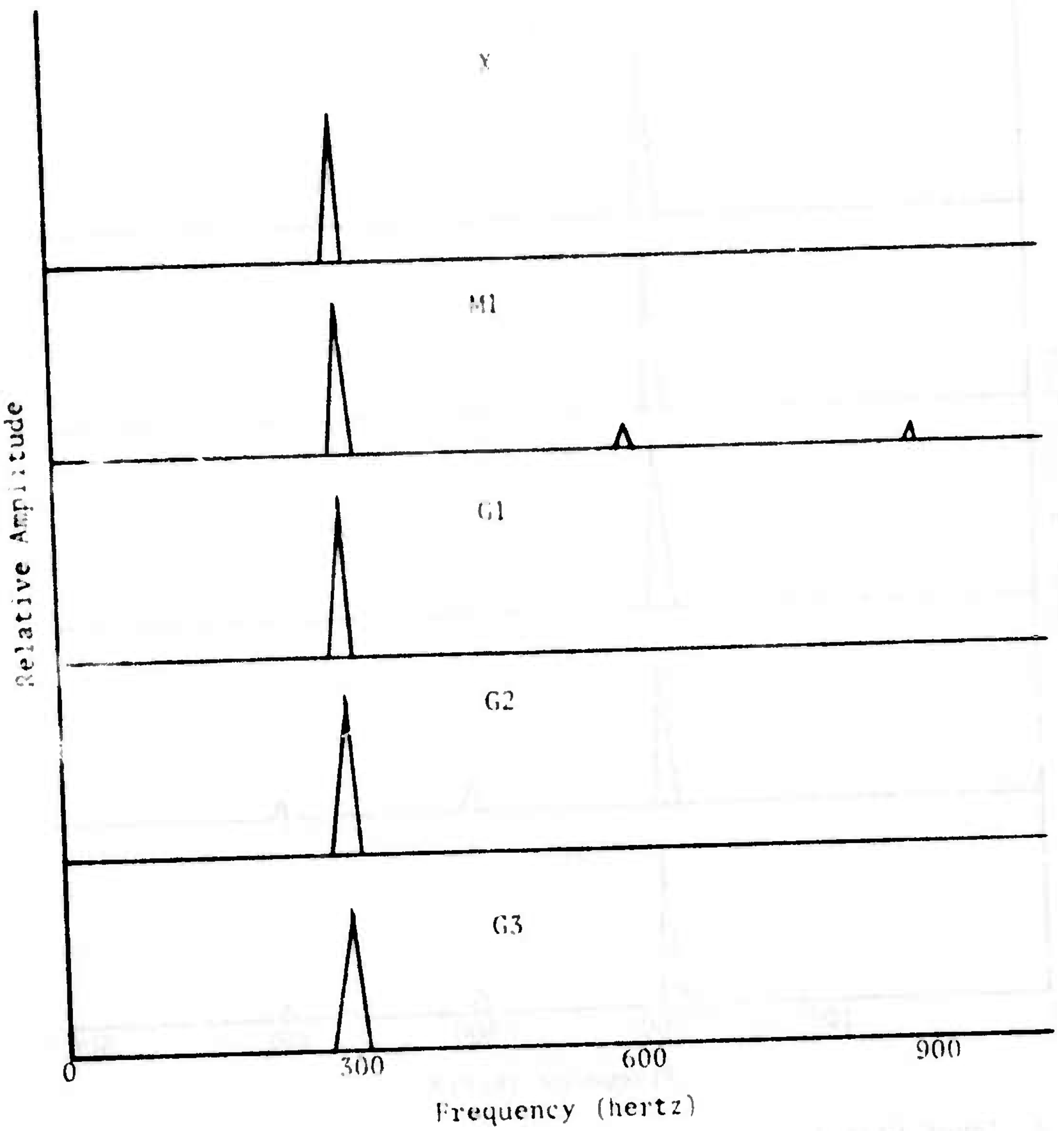

X Input Signal
M1 Signal at Microphone 1
G1 Signal at Geophone 1
G2 Signal at Geophone 2
G3 Signal at Geophone 3

Figure 7. System Harmonics at 300-Hertz Input

it can be seen from Figure 5 that the third harmonic has very little energy compared to the second harmonic and the fundamental at 100 hertz. At 200 hertz (Figure 6) the third harmonic in the geophone signal is not detectable. This analysis indicates that if the audio system could be separated from the seismic system there would be very little total energy contribution gained from computation of a third order kernel.

Figure 8 is a plot of the relative shapes of the PSD of the system signals taken from the spectrum analyzer. The speaker output (M1) is obviously nonwhite and therefore does not qualify as a proper input for identifying a nonlinear system. If the speaker system were linear, the seismic system could still be identified simply by using the input from the noise generator and dividing out the speaker transfer function, i.e.,

$$H_1(f) = \frac{Y(f)X^*(f)}{S(f)} \tag{16}$$

and

$$H_2(f_1,f_2) = \frac{Y(f_1 + f_2)X^*(f_1)X^*(f_2)}{2A^2S(f_1)S(f_2)} \tag{17}$$

where H_1 and H_2 are the first and second order kernels of the seismic medium and S(f) is the speaker transfer function. Since the speaker system is obviously nonlinear because of the appearance of the harmonics in the speaker output, the above procedure does not work.

Since the signal at G1 is also nonwhite and nonlinear, the same analysis applies.

Therefore, it must be concluded that the transfer characteristics of the seismic/acoustic medium cannot be determined by this method with the equipment available. Only the total system, including the audio system and the transfer medium, can be evaluated. The analysis was continued in the interest of checking out the mathematical computation procedures while continuing a search for better equipment.

Evaluation of system response to impulsive inputs which impart acoustic as well as seismic energy to the system gives some indication of system memory which, in turn, indicates the temporal record length required to adequately characterize the system. Such inputs are created by striking a metal plate with a hammer. The acoustic wave which travels through the atmosphere is the first signal to be detected by the geophone. The hammer blow also generates a compression wave which propagates into the surface and a shear wave which travels along the surface. The Rayleigh wave which is the vector sum of the compression and shear waves (White, 1965) is the last disturbance registered by the geophone. The system memory is then defined as approximately the time interval $t_2 - t_1$, where t_2 is time of arrival of the Rayleigh wave and t_1 is the time of arrival of the acoustic wave.

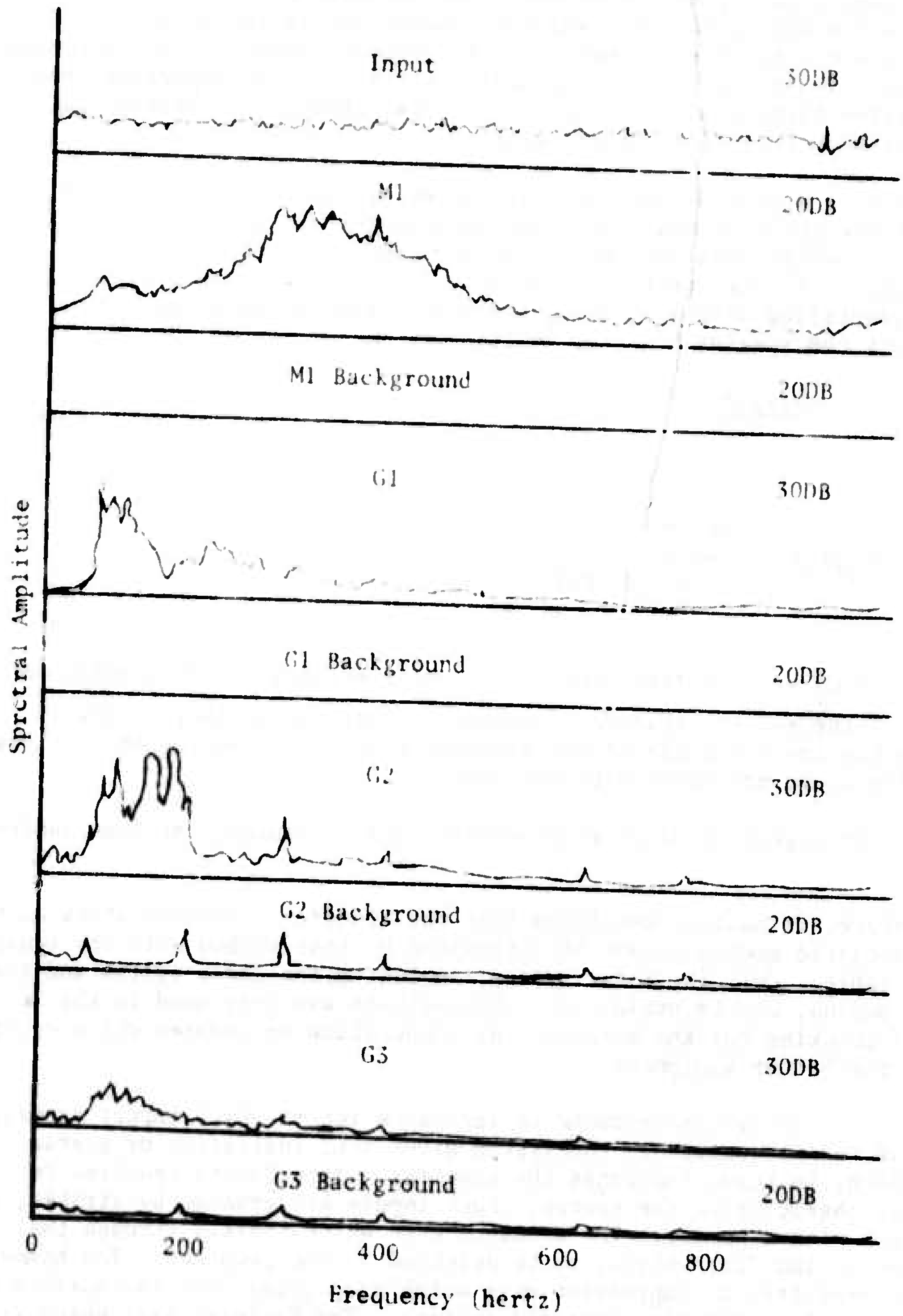

Figure 8. Relative Shape of Power Spectral Density of System Signals and Background Noise

The acoustic wave travels at about 1100 feet per second in a no-wind condition. The Rayleigh wave velocity varies from 500 to 1000 feet per second depending on soil conditions. Analysis of the impulse responses indicated that the Rayleigh wave was traveling at about 550 feet per second during these experiments. At a distance of 10 feet, the system memory would then be about 0.01 second.

According to Marmarelis (1972), the data record length, R, should be

$$R = \text{MAX}\left[\frac{1}{f_n}, t_2 - t_1\right] M \tag{18}$$

where f_n is the Nyquist sampling rate. M, the number of independent samples, should be at least 100 to reduce the error caused by a finite record length to 5 percent. This indicates that a one-second data interval is required for the computation of a kernel at 10 feet. As the distance is increased, the memory increases up to a point where pure acoustic energy is no longer detected by the geophone.

COMPUTATION OF THE KERNELS

A first and second order kernel was computed for the total system from noise generator to geophone G2 located 10 feet from the speaker. One-eighth second data sequences were used, and the ensemble average was taken over 40 samples. The kernels therefore represent 5 seconds of independent data.

For purposes of comparison a linear transfer function was computed for the same system using the relation

$$L(f) = \frac{Y(f)}{X(f)} \tag{19}$$

where L(f) is denoted here as the linear filter. The linear filter was used as a method of comparing the ability of the kernels to predict an output for a given input.

The magnitude of the transformed first order kernel is shown in Figure 9. The linear filter is shown in Figure 10. For a linear system the first order kernel and the linear filter are identical. For a nonlinear system of order three or higher, however, G_3, G_5, and all odd order G-functionals contain a linear term which contributes to the total linear portion of the output.

The magnitude of the transform of second order kernel is shown in Figure 11. Phase information was not plotted but was carried in the computer. Some savings in computation time can be realized by recognizing the symmetries in the second order kernel. From Equation (13) it is seen that $H_2(f_1,f_2) = H_2(f_2,f_1)$. Therefore the function is symmetrical about the

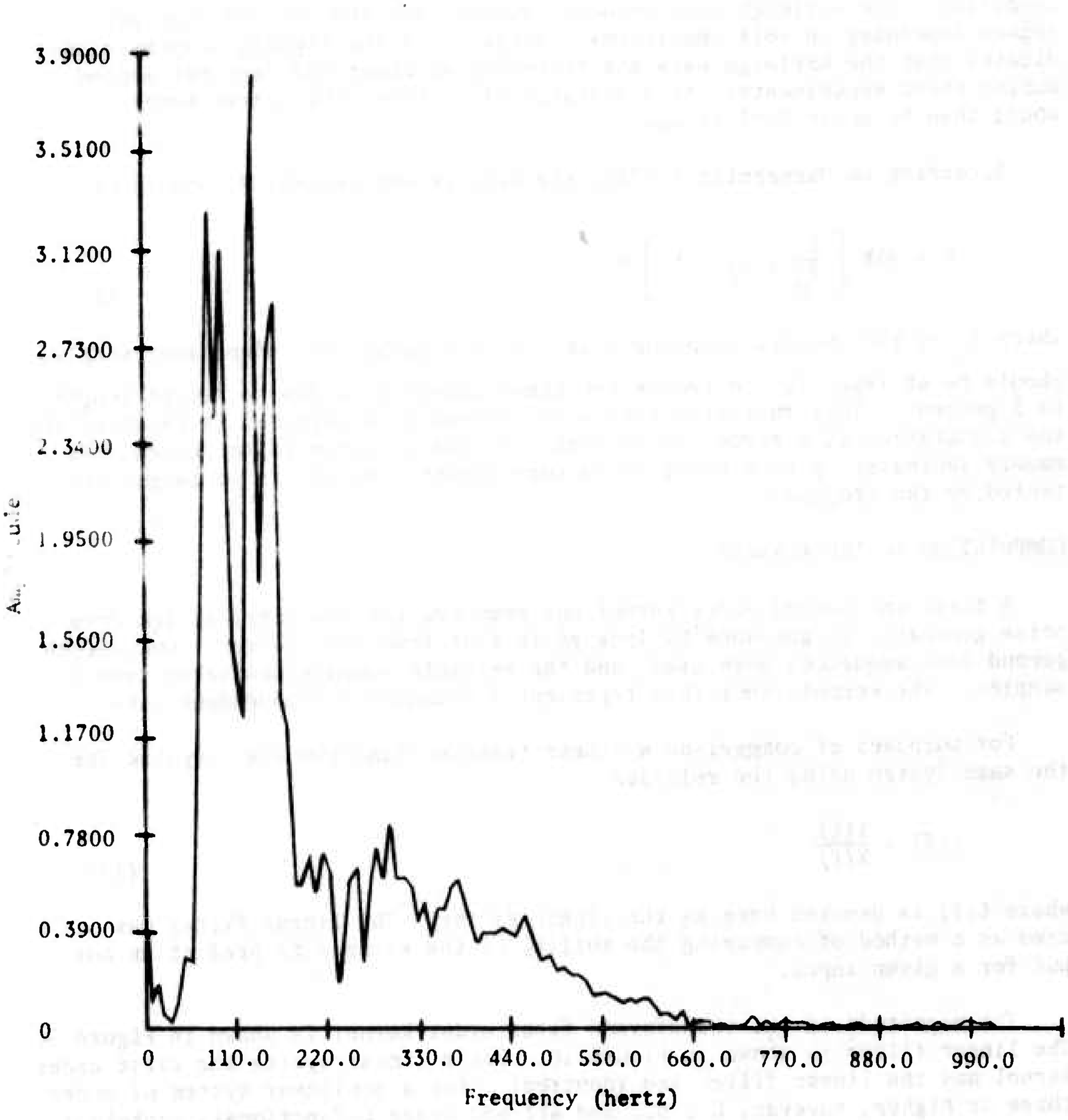

Figure 9. First Order Wiener Kernel

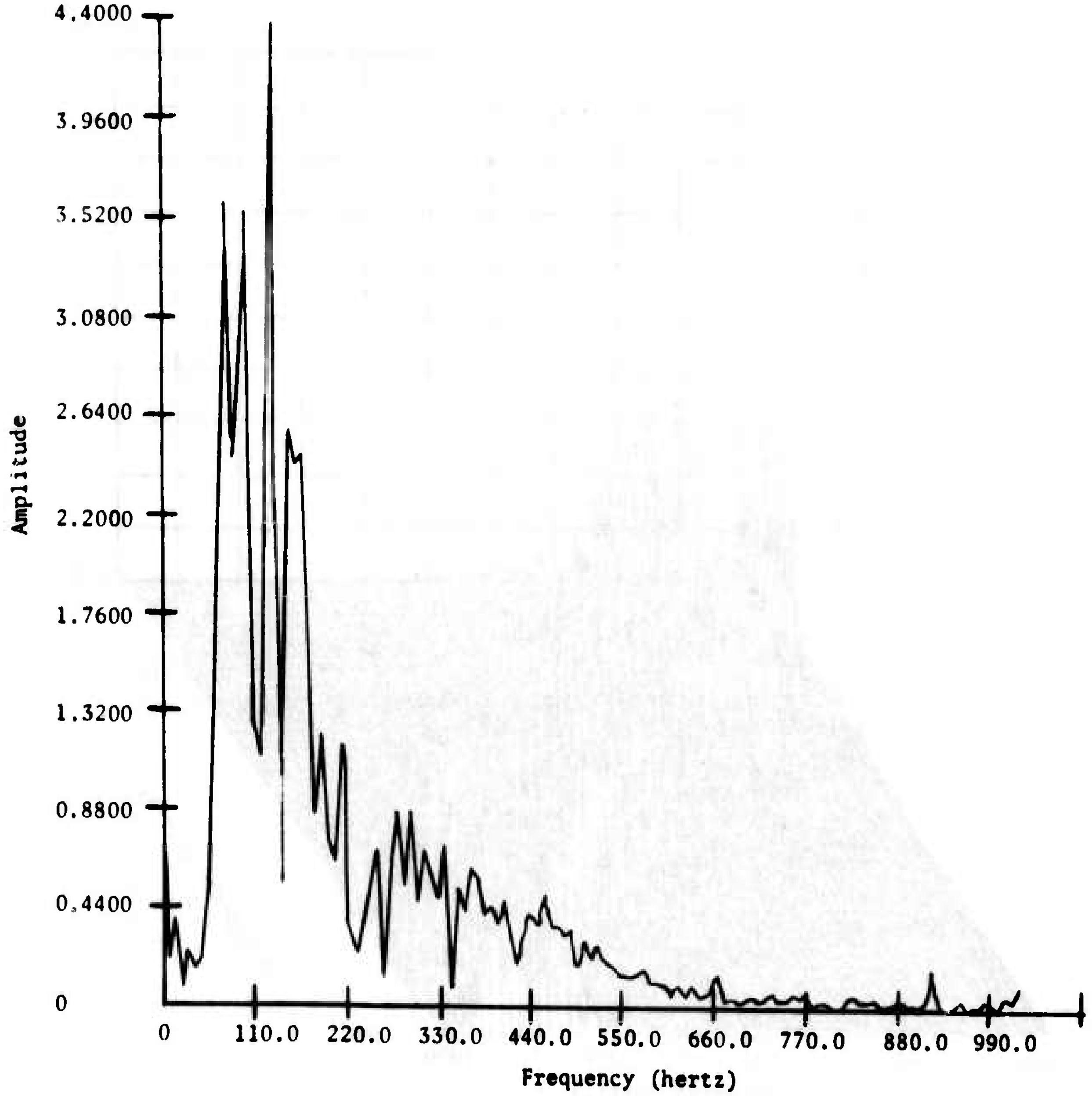

Figure 10. Linear Filter

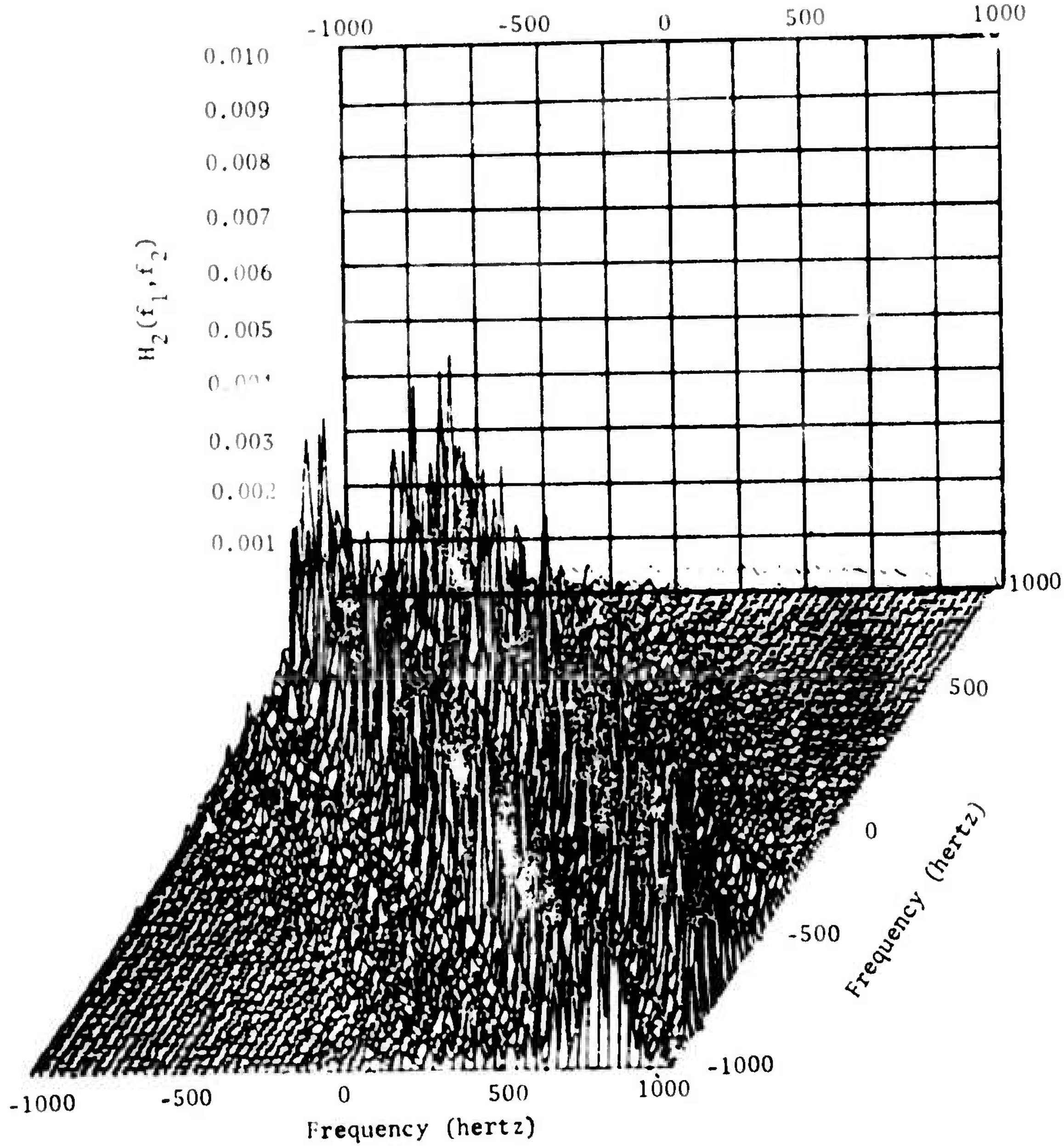

Figure 11. Second Order Wiener Kernel

line $f_1 = f_2$. In addition, H_2 has conjugate symmetry, i.e., $H_2(f_1,f_2) = H_2^*(-f_1, -f_2)$, which follows from the fact that $h_2(\tau_1,\tau_2)$ is real. Also, $H_2(f_1,f_2)$ is zero for $|f_1 + f_2| > 1000$ because values for Y(f) are nonzero only in the range $|f| < 1000$. Using the above symmetry, $H_2(f_1,f_2)$ is completely determined by its values in Areas 1 and 2, as shown in Figure 12.

In order to evaluate the derived model, the kernels were used to compute an expected output for a given input signal. The computed output was compared with the output measured at G2 for the same input signal. Equation (11) was used to compute the output.

At this point it is noted that the sensors used in this experiment are not capable of measuring a direct current signal. Therefore, $h_0 = \overline{y(t)}$ is considered to be zero throughout the computation. This means that the second term of the second-order kernel

$$h_0\delta\left(f_1 + f_2\right) = 0$$

and also the second term of the second order G-functional,

$$A\int_{-\infty}^{\infty} H_2(f, -f)df = \frac{1}{2A}\int_{-\infty}^{\infty} \langle Y(0)X(f)X(-f)\rangle df = 0$$

since $\langle Y(0)\rangle = H_0 = 0$. The expression for y(t), the computed output reduces to

$$y(t) = G_1(t) + G_2(t) \tag{20}$$

where $G_1(t)$ is the contribution of the first order kernel and $G_2(t)$ is the contribution of the second order kernel.

The comparisons were made by cross-correlating the measured output signal with the computed outputs. Figure 13 shows the autocorrelation of the measured output at G2 compared with the cross-correlations of the output and that computed from $H_1(f)$ alone, and then the output and that computed from both $H_1(f)$ and $H_2(f_1,f_2)$. Figure 14 shows the same comparison between the output computed from $H_1(f)$, that computed from L(f), and the autocorrelation of the measured signal. A second comparison of the outputs can be made from the PSD plots of Figures 15 through 18 and Figure 19 which compares the integrated power of the output signals. These comparisons show

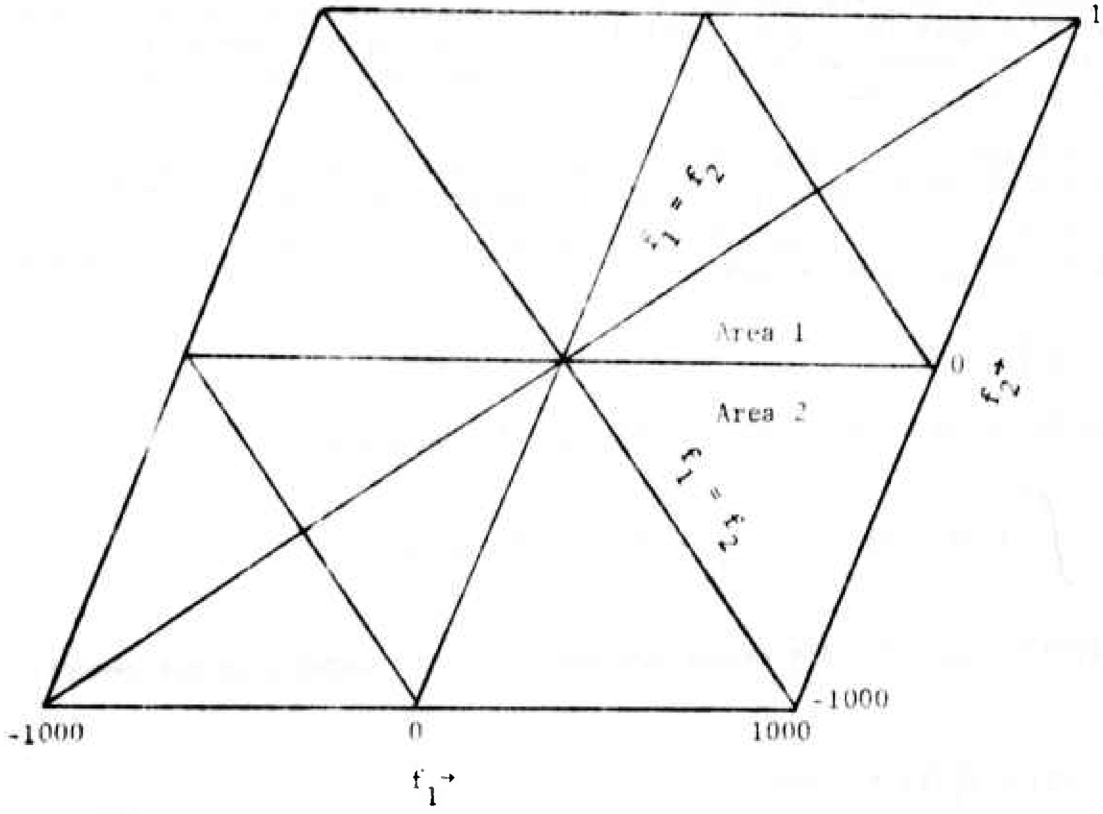

Figure 12. Diagram Depicting Areas of Symmetry in the f_1/f_2 Plane of the Second Order Kernel

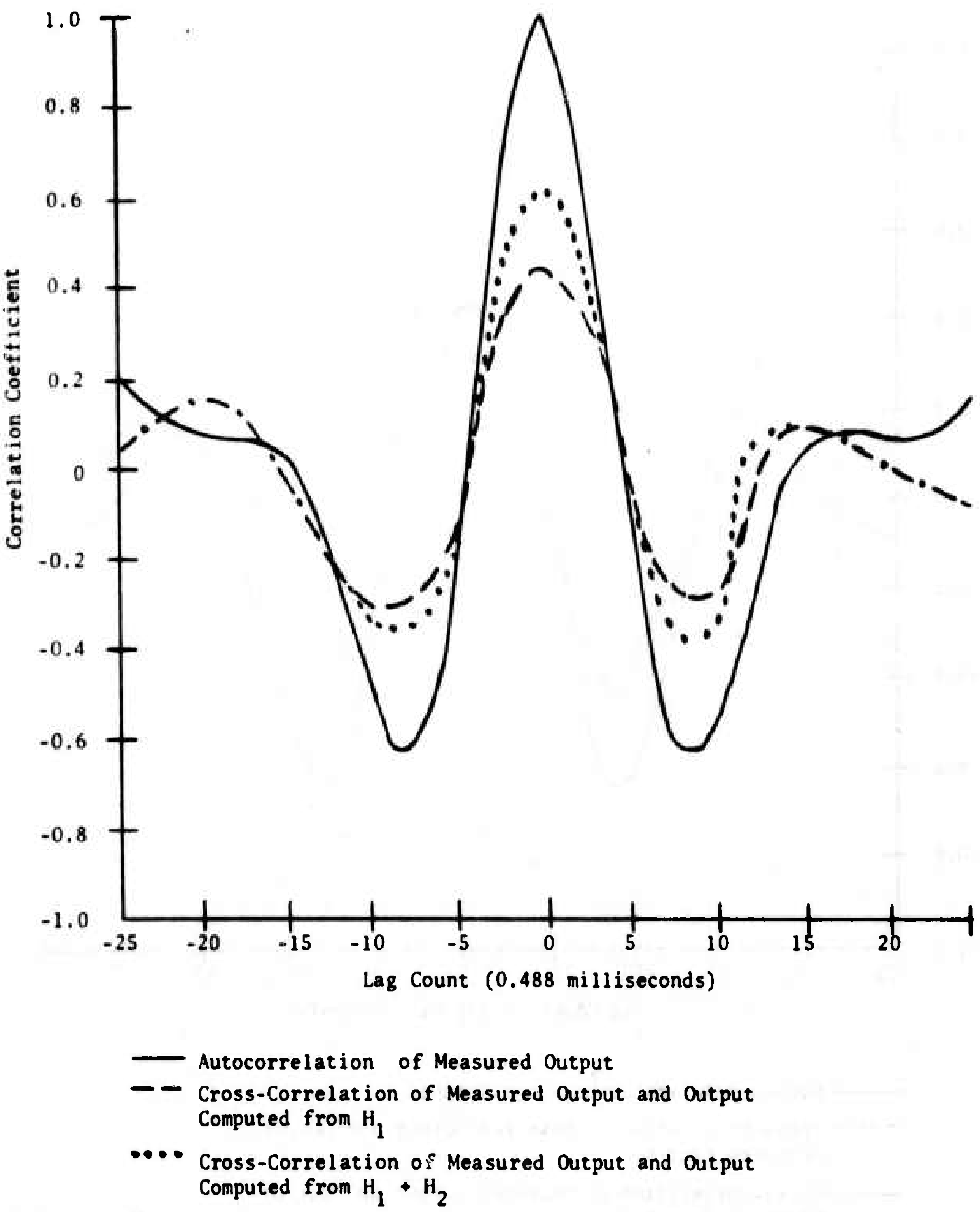

Figure 13. Correlation Coefficients of Computed versus Measured Output

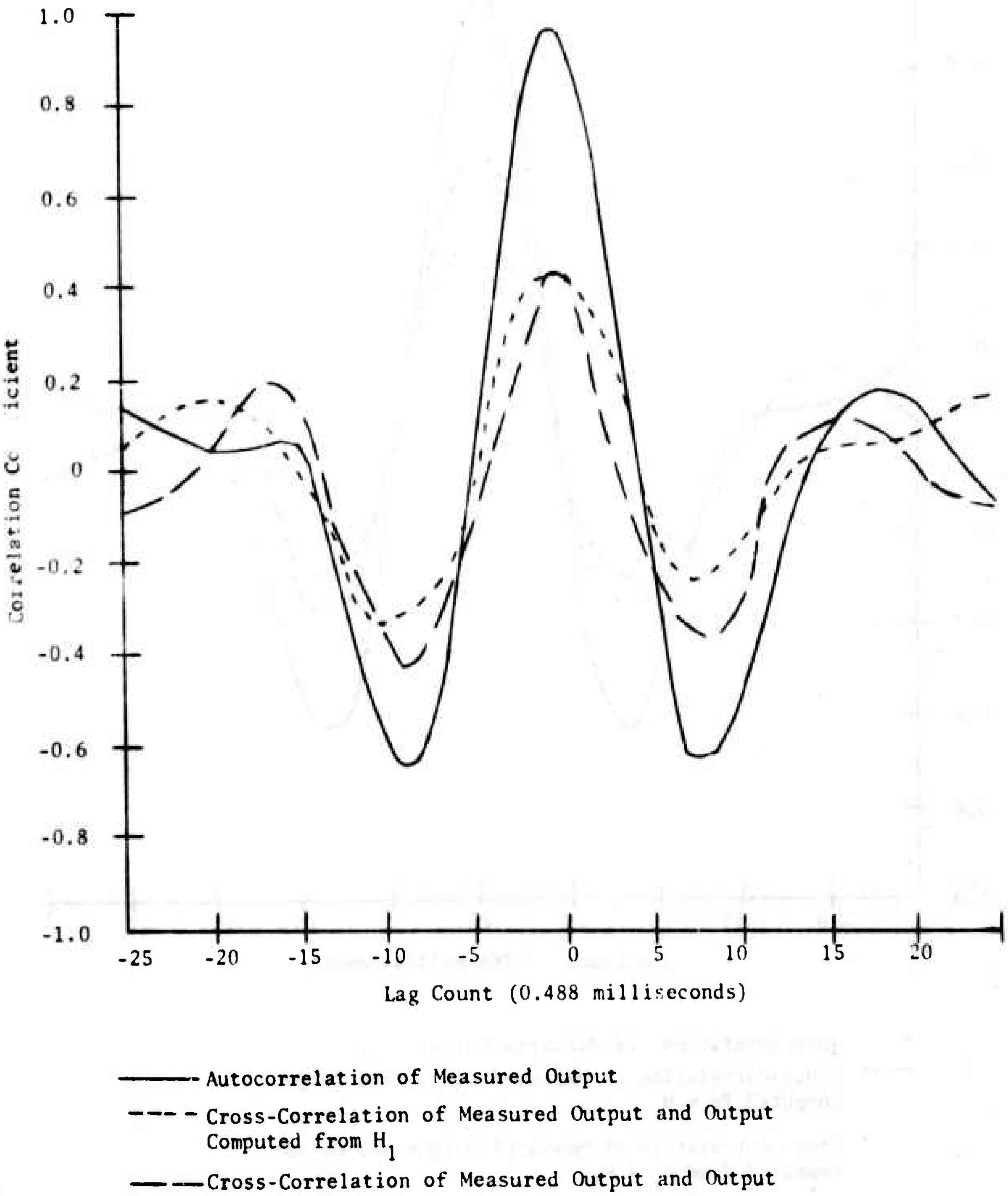

Figure 14. Comparison of Output Computed from First Order Kernel and Output Computed from Linear Filter

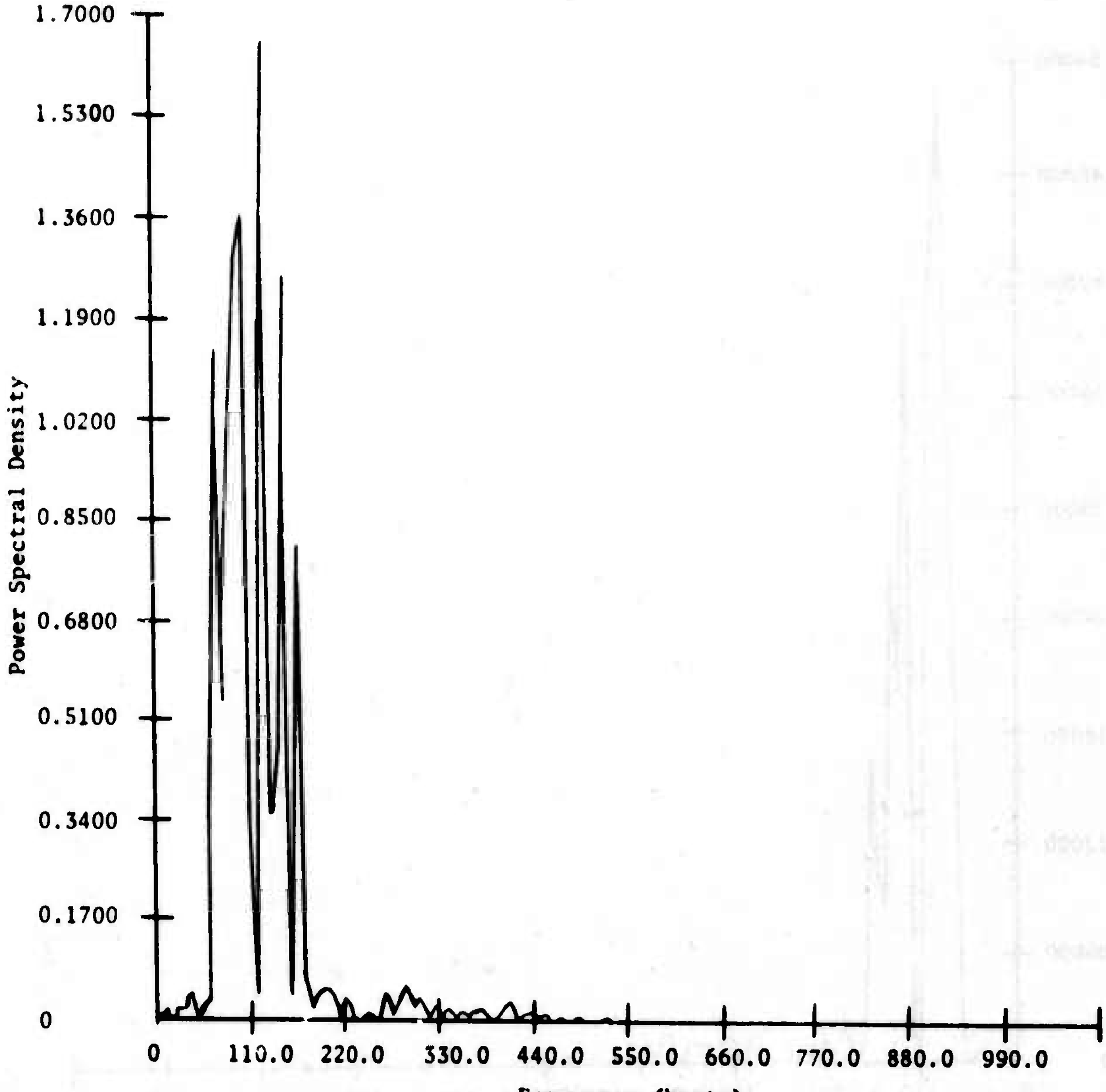

Figure 15. Power Spectral Density of Measured Output

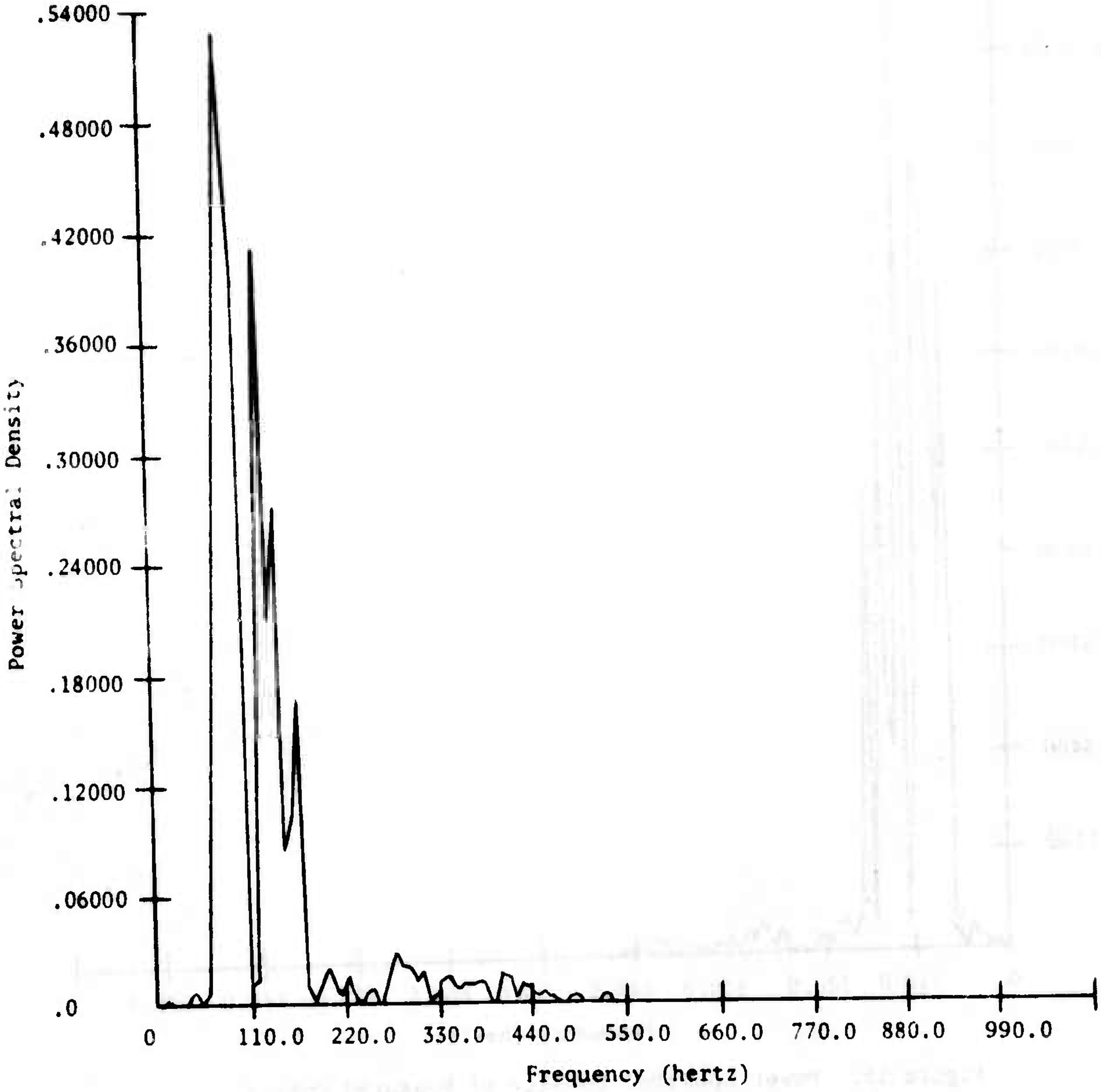

Figure 16. Power Spectral Density of Output
Computed from First Order Kernel

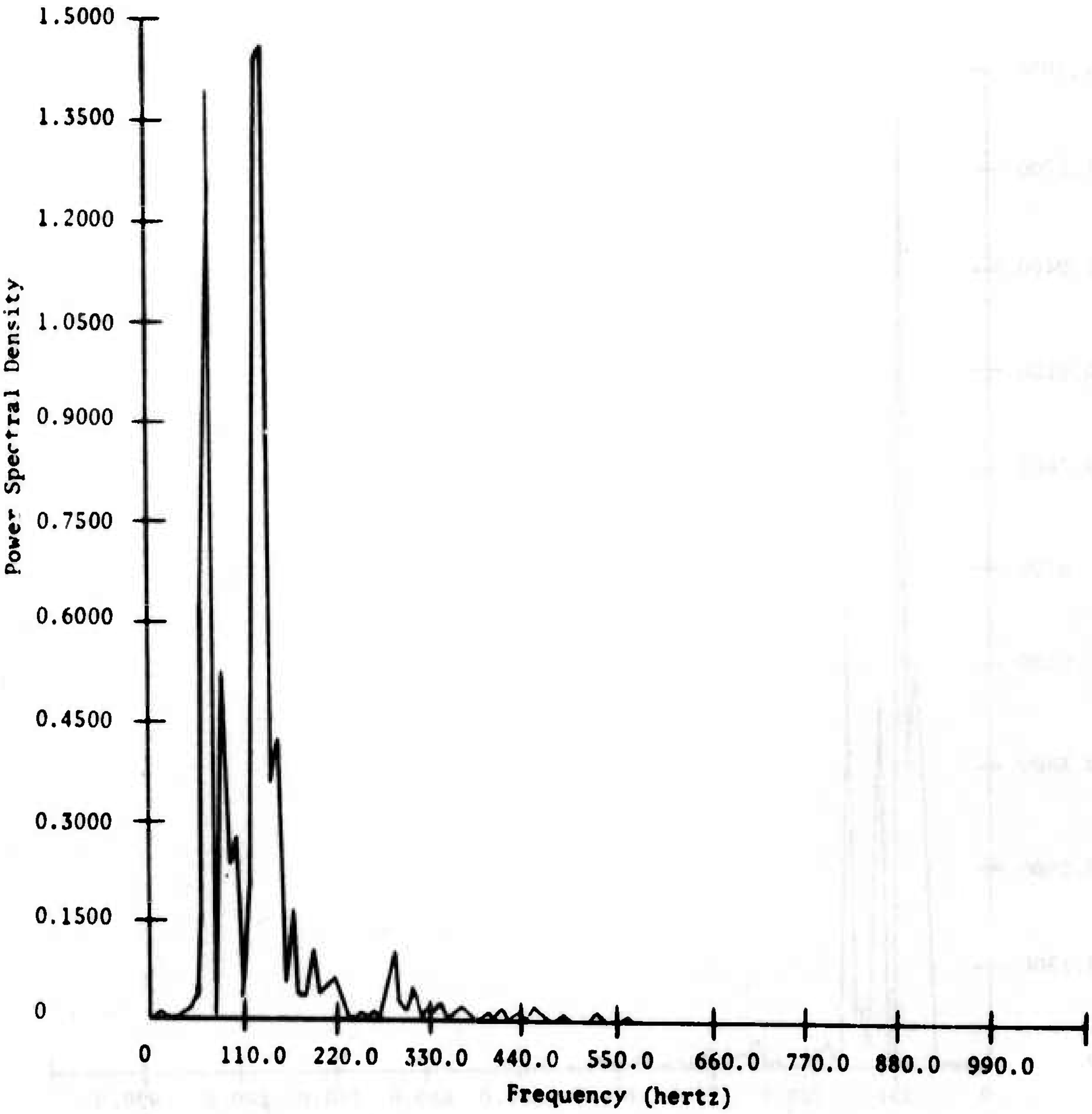

Figure 17. Power Spectral Density of Output Computed from First and Second Order Kernels

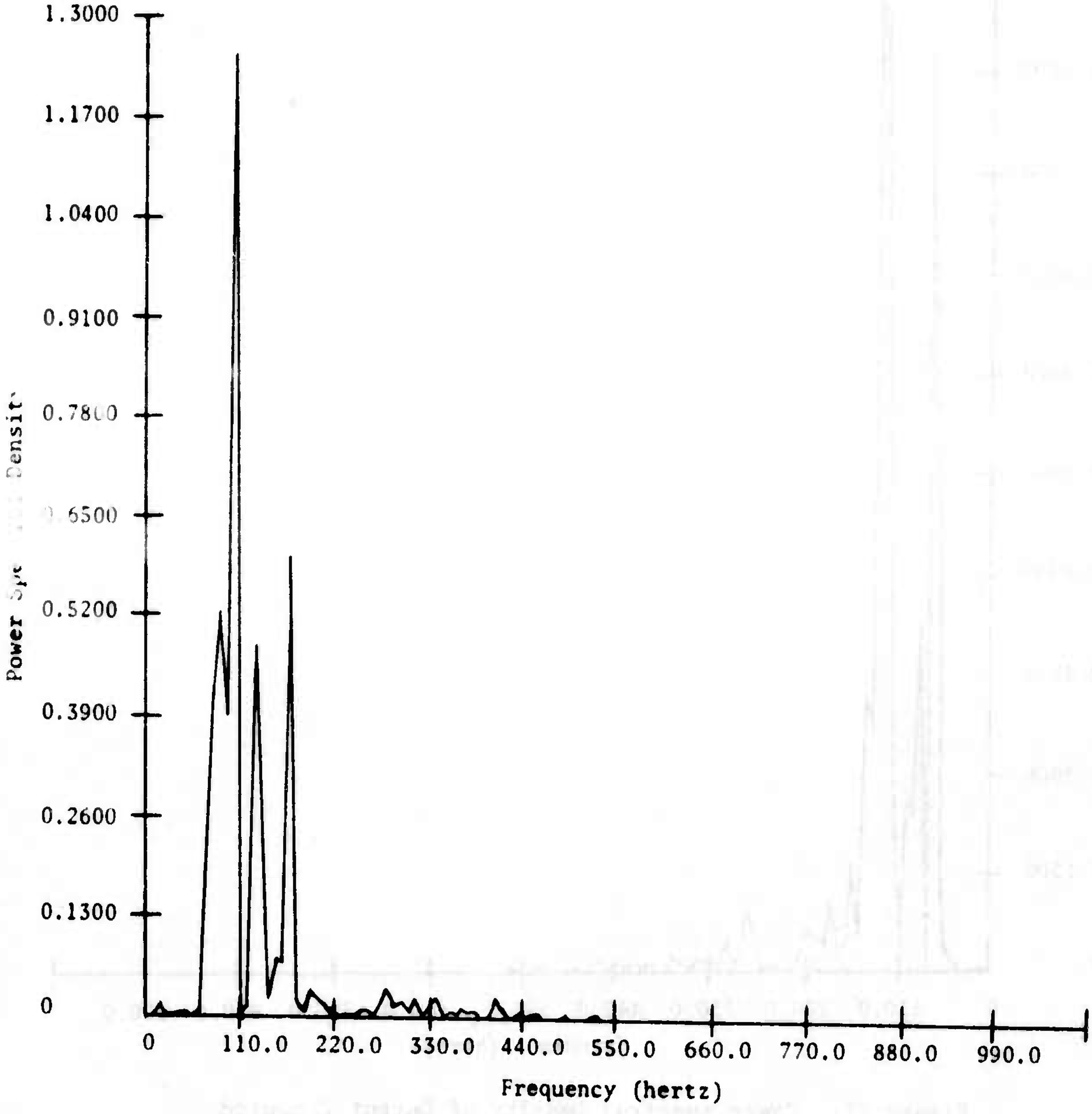

Figure 18. Power Spectral Density of Output Computed from Linear Filter

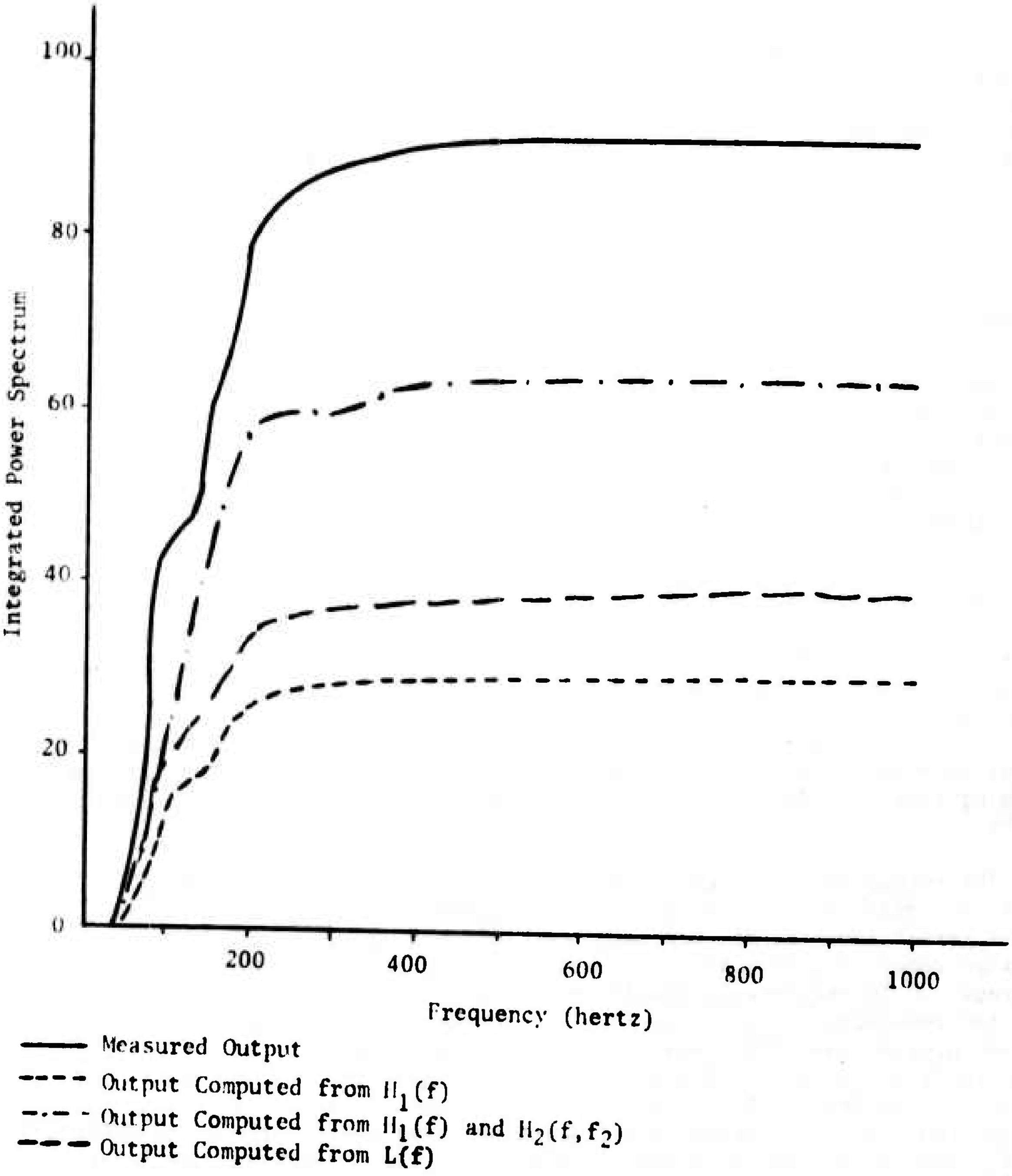

Figure 19. Integrated Power Spectrum of Measured and Computed Outputs

that the output computed with the first and second order kernel give a much better representation of the measured signal than the output computed by linear procedures. Use of the second order kernel improves the correlation between computed and measured output by about 45 percent over that computed from $H_1(f)$ alone. From Figure 19, it is seen that there is still energy unaccounted for even when the outputs from $H_1(f)$ and $H_2(f_1,f_2)$ are combined. This is probably attributable to the third and fourth order nonlinearities which were observed in Figure 4.

COMPUTATION PROBLEMS

The requirement for ensemble averaging makes the Fourier transform method of computing the kernels much less attractive than originally anticipated. Computing time is increased directly with the number of data sequences used in the ensemble. Also, there is no good standard available to judge the number of samples required to produce an acceptable measure of accuracy. When these factors are considered, the cross-correlation method in time domain begins to look more attractive.

Although computing time is expensive, this is not the primary problem on the CDC 6600 computer. The primary consideration in this program is storage. The CDC 6600 computer used in this computation limits each program to 32,000 words in the core and two million words on disk storage. Of course, tape storage could be used, but when more than one tape is required to hold one kernel, the program must be interrupted to change the tapes. This, in turn, increases running time. Routine programs which exceed 10 to 15 minutes running time have difficulty in being scheduled for the computer except at night.

The second order kernel in frequency domain requires $2n^2$ storage locations where n is the number of data samples. In addition, the first order kernel requires 2n, and each time sequence used in the ensemble average requires n locations. A half-second of our data with 40 ensemble averages would require all available disk and core storage leaving no room for the remainder of the program. This storage limitation can be overriden if the program has sufficient priority. A second possibility is to reduce the digitization rate. As can be seen from Figure 16, most of the output energy is confined to the 0- to 300-hertz frequency band. As pointed out in Section III, input noise data samples are available in the 2- to 300-hertz band. This data could be redigitized at a 600-hertz sampling rate which would then better allow us to use a longer data sequence in each ensemble.

SECTION V

CONCLUSIONS

This research has been a first attempt to analyze the seismic/acoustic transfer problem using the Wiener theory of nonlinear systems. The research has proven to be very valuable in that it has shown conclusively that the system is nonlinear, and linear procedures are not adequate for modeling the system.

The primary problem area in this experiment was the failure of the equipment to respond in the frequencies below 60 hertz. The targets of interest for which these transfer functions are required transmit direct and acoustically coupled seismic energy of significant amplitude in the frequency range of 5 to 100 hertz (Constantine and Walker, 1976).

The equipment used in this research provided no information below 60 hertz. Also due to the nonlinearity of the speaker, the system analyzed was not the seismic medium but the total system, including the audio system and the seismic medium.

Currently a search is underway to find a ground-vibrating system which will respond in the frequency band of 5 to 100 hertz. Ideally, this system should generate ground vibrations as well as acoustic signals.

Secondly, a better means of measuring the system input must be devised. In this research neither the microphone nor the geophone provided a complete measure of the system input. The microphone will not measure direct ground vibrations while the geophone, placed beneath the speaker, is bypassed by much of the acoustic energy. Probably the best measure of system input would be obtained by a geophone rigidly attached to the vibrator.

If the above equipment problems can be solved and a means of making a linear transfer of energy from the noise generator to the medium devised, it is very likely that the third and fourth harmonics observed in this research will disappear. Then the system can be adequately characterized by the first and second order kernels developed here.

SECTION VI

RECOMMENDATIONS

It is recommended that:

1. The effort be continued to locate an earth vibrator which will respond in the frequency range of 5 to 100 hertz and make a linear transfer of energy from the noise generator to the ground.

2. The computing efforts with the data currently on hand be continued in the frequency band of 0- to 300-hertz to refine the frequency domain method of computation.

3. Concurrently with frequency domain calculations, a program should be initiated to calculate the kernels in time domain to provide a means of checking computational efficiency, numerical accuracy, and stability of the frequency domain methods.

4. A program be initiated to compute the kernels as a function of distance.

BIBLIOGRAPHY

Bendat, J.S., and A.G. Piersol, Random Data: Analysis and Measurement Procedures, Wiley-Interscience, New York, 1971.

Bingham, Christopher, Michael D. Godfrey, and John W. Tukey, "Modern Techniques of Power Spectrum Estimation," IEEE Transactions on Audio and Electro-Acoustics, Vol. AU-15, No. 2, June 1967, pp. 56-66.

Childers, Donald, and Allen Durling, Digital Filtering and Processing, West Publishing Company, St. Paul, 1975.

Cochran, William T., with G-AE Subcommittee on Measurement Concepts, "What is the Fast Fourier Transform?" IEEE Transactions on Audio and Electro-Acoustics, Vol. AU-15, No. 2, June 1967, pp. 45-55.

Constantine, J.G., and R.B. Walker, Seismic/Acoustic Signature Characterization for Classification and Ranging, paper presented at Second Symposium on the Design, Testing, and Deployment of Unattended Ground Sensors, Waterways Experiment Station, Vicksburg, Mississippi, April 1976.

Cooley, J.W., P.A.W. Lewis, and P.D. Welch, "Application of the Fast Fourier Transform to Computation of Fourier Integrals, Fourier Series, and Convolution Integrals," IEEE Transactions on Audio and Electro-Acoustics, Vol. AU-15, No. 2, June 1967, pp. 79-84.

Cooley, J.W., and J.W. Tukey, "An Algorithm for the Machine Calculation of Complex Fourier Series," Mathematics of Computation, Vol. 19, 1965, pp. 297-301.

Crawford, J.M., W.E.N. Doty, and M.R. Lee, "Continuous Signal Seismograph," Geophysics, Vol. XXV, No. 1, February 1960, pp. 95-105.

Fisher, James R., NRL Report 7041, Fortran Program for Fast Fourier Transform, Naval Research Laboratory, Washington, D.C., April 1970.

French, A.S., and E.G. Butz, "Measuring the Wiener Kernels of a Nonlinear System Using the Fast Fourier Transform," Int. J. Control, Vol 17, No. 3, 1973, pp. 529-539.

French, A.S., and A.V. Holden, "Alias-Free Sampling of Neuronal Spike Trains," Kybernetik, Vol. 8, 1971, pp. 165-171.

French, A.S., and A.V. Holden, "Semi-on-Line Implementation of an Alias-Free Sampling System for Neuronal Signals," Computer Programs in Biomedicine, Vol. 2, 1971, pp. 1-7.

Helms, H.D., "Fast Fourier Transform Method of Computing Difference Equations and Simulating Filters," IEEE Transactions on Audio and Electro-Acoustics, Vol. AU-15, No. 2, June 1976, pp. 85-90.

Hemdal, J.F., An Investigation of Automatic Identification of Acoustic and Seismic Sources, BRL-CR-86, Willows Run Laboratories, Institute of Science and Technology, The University of Michigan, Ann Arbor, Michigan for USA Ballistic Research Laboratories, Aberdeen Proving Ground, Maryland, February 1973.

Lee, Y.W. "Contributions of Norbert Wiener to Linear Theory and Nonlinear Theory in Engineering," from Selected Papers of Norbert Wiener, S.I.A.M. and M.I.T. Press, Cambridge, 1964, pp. 17-33.

Lee, Y.W., Statistical Theory of Communications, Wiley, New York, 1960.

Lee, Y.W., and M. Schetzen, "Measurement of the Wiener Kernels of a Nonlinear System by Cross-Correlation," Int. J. Control, Vol. 2, 1965, pp. 237-254.

Lundien, J.R., Terrain Constraints on the Design Testing and Development of the Gator Mine, ADTC-TR-75-15 (AFATL-TR-75-57), Mobility and Environmental Systems Laboratory, U.S. Army Engineer Waterways Experiment Station, Vicksburg, Mississippi, for Munitions SPO, Deputy for Armament Systems, Armament Development and Test Center, Eglin Air Force Base, Florida, March 1975.

Lundien, J.R., and H. Nikodem, A Mathematical Model for Predicting Micro-Seismic Signals in Terrain Materials, Technical Report M-73-4, U.S. Army Engineer Waterways Experiment Station, Vicksburg, Mississippi, June 1973.

Marmarelis, P.Z., "Nonlinear Identification of Bioneuronal Systems Through White-Noise Stimulation," Proceedings of the Joint Automatic Control Conference, Stanford University, August 1972, pp. 117-126.

Marmarelis, P.Z., and K.I. Naka, "White-Noise Analysis of a Neuron Chain: An Application of the Wiener Theory," Science, Vol. 175, No. 4027, 17 March 1972, pp. 1276-1278.

Marmarelis, P.Z., and G.D. McCann, "Development and Application of White-Noise, Modeling Techniques for Studies of Insect Visual Nervous System," Kybernetik, Vol. 12, pp. 74-89.

McCann, G.D., "Nonlinear Identification Theory Models for Successive Stages of Visual Nervous Systems of Flies," J. Neurophysiology, Vol. 37, 1974, pp. 869-895.

Papoulis, A., Probability, Random Variables, and Stochastic Processes, McGraw-Hill, New York, 1965.

Schwartz, Mischa, and Leonard Shaw, Signal Processing - Discrete Signal Analysis, Detection, and Estimation, McGraw-Hill, New York, 1975.

Singleton, R.C., "A Method for Computing the Fast Fourier Transforms with Auxiliary Memory and Limited High-Speed Storage," IEEE Transactions on Audio and Electro-Acoustics, Vol. AU-15, No. 2, June 1967, pp. 91-98.

Volterra, V., The Theory of Functionals and Integro-differential Equations, Blackie, London, 1930.

White, J.E., Seismic Waves: Radiation, Transmission, and Attenuation, McGraw-Hill, New York, 1965.

Wiener, N., Nonlinear Problems in Random Theory, M.I.T. Press, Cambridge, 1958.

(The reverse of this page is blank)

APPENDIX A

DATA RECORD

Each signal is identified by a 5-digit number. The first digit is the number of the analog tape; the second and third digits represent experiment number (01 through 12); the fourth digit represents signal type (0 for background, 1 for sweep time, 2 for noise, 3 for vehicle data); and the fifth digit is a chronological signal within each type. Digital data may be called by signal number. Analog data may be located by its time-coded location on the tape.

Tape 1

SIGNAL NO.	TIME CODE	DESCRIPTION
10101	22:33:00-22:34:00	Background
10111	22:40:23-22:40:33	30-50 Hz Sweep
10112	22:41:47-22:41:57	50-100 Hz Sweep
10113	22:43:50-22:44:00	100-200 Hz Sweep
10114	22:44:50-22:45:00	200-500 Hz Sweep
10115	22:46:10-22:46:20	500-1000 Hz Sweep
10116	22:47:42-22:47:52	1000-200 Hz Sweep
10117	22:48:57-22:49:07	1000-100 Hz Sweep
10102	22:49:30-22:50:15	Background
10121	22:50:30-22:52:30	0-2 KHz Noise
10122	22:53:00-22:54:30	0-1 KHz Noise
10123	22:56:00-22:57:30	0-500 Hz Noise
10103	22:58:00-22:59:00	Background
10131	22:59:16-22:59:36	Vehicle Engine Idle
10132	23:00:50-23:01:10	Vehicle Fast Idle
10133	23:02:13-23:02:20	Vehicle Power off Pass
10134	23:02:56-23:03:26	Vehicle Power on Pass
10201	23:08:00-23:08:30	Background
10211	23:14:20-23:14:30	30-50 Hz Sweep
10212	23:15:43-23:15:53	50-100 Hz Sweep
10213	23:17:35-23:17:45	100-200 Hz Sweep
10214	23:19:07-23:19:17	200-100 Hz Sweep
10215	23:19:37-23:19:47	100-500 Hz Sweep
10216	23:21:37-23:21:47	500-1000 Hz Sweep
10202	23:25:00-23:25:30	Background
10221	23:26:00-23:27:30	0-2 KHz Noise
10222	23:28:00-23:29:30	0-500 Hz Noise
10223	23:29:40-23:31:00	0-200 Hz Noise
10224	23:31:10-23:31:55	0-100 Hz Noise
10225	23:32:40-23:33:25	200-300 Hz Noise

SIGNAL NO.	TIME CODE	DESCRIPTION
10301	23:40·05-23:50:00	Background
10311	23:42:22-23:42:32	30-50 Hz Sweep
10312	23:44:20-23:44:30	50-100 Hz Sweep
10313	23:47:07-23:47:17	100-200 Hz Sweep
10314	23:49:08-23:49:18	300-500 Hz Sweep
10315	23:50:25-23:50:35	500-1000 Hz Sweep
10316	23:51:53-23:52:03	1000-700 Hz Sweep
10302	23:54:00-23:54:30	Background
10321	23:55:00-23:56:30	0-2 KHz Noise
10322	23:56:45-23:57:45	0-500 Hz Noise
10323	23:58:00-23:59:30	0-200 Hz Noise
10324	00:00:00-00:01:30	0-100 Hz Noise
10325	00:02:00-00:03:30	200-300 Hz Noise
10303	00:08:00-00:08:30	Background
10331	00:14:00-00:14:30	Vehicle Idle
10332	00:16:00-00:16:30	Vehicle Fast Idle
10333	00:17:20-00:17:30	Engine Off Pass
10334	00:18:20-00:18:30	Engine On Pass
10401	00:19:30-00:20:10	Background
10402	00:21:30-00:22:00	Background (Aircraft)
10411	00:28:35-00:28:45	30-50 Hz Sweep
10412	00:29:30-00:29:40	50-100 Hz Sweep
10413	00:31:00-00:31:10	100-20 Hz Sweep
10414	00:34:00-00:34:10	60-500 Hz Sweep
10415	00:35:40-00:35:50	500-1000 Hz Sweep
10403	00:37:00-00:37:30	Background
10421	00:43:00-00:43:30	0-2 KHz Noise
10422	00:44:30-00:45:30	0-500 Hz Noise
10423	00:46:30-00:47:15	0-200 Hz Noise
10424	00:47:45-00:48:30	0-100 Hz Noise
10425	00:48:40-00:49:30	200-300 Hz Noise
10511	00:51:15-00:51:25	30-50 Hz Sweep
10512	00:52:30-00:52:40	50-100 Hz Sweep
10513	00:55:05-00:55:15	1000-200 Hz Sweep
10514	00:56:30-00:56:40	200-500 Hz Sweep
10515	00:57:55-00:58:05	500-1000 Hz Sweep
10516	00:59:05-00:59:15	1000-200 Hz Sweep
10521	01:20:45-01:21:15	0-2 KHz Noise
10522	01:23:20-01:23:40	0-500 Hz Noise
10523	01:25:40-01:26:10	0-200 Hz Noise
10524	01:28:00-01:28:30	0-100 Hz Noise
10525	01:29:30-01:30:00	200-300 Hz Noise
10531	01:31:30-01:32:00	Vehicle Idling
10532	01:34:10-01:34:20	Vehicle Exhaust
10533	01:34:10-01:34:20	Engine on Pass
10534	01:34:35-01:34:45	Engine on Pass
10535	01:35:00-01:35:10	Engine Off Pass
10536	01:35:30-01:35:40	Engine Off Pass

Tape 2

SIGNAL NO.	TIME CODE	DESCRIPTION
20611	04:27:45-04:27:55	100-30 Hz Sweep
20612	04:28:55-04:29:05	30-50 Hz Sweep
20613	04:29:10-04:29:20	50-100 Hz Sweep
20614	04:29:40-04:30:10	1000-100 Hz Sweep
20615	04:31:10-04:31:30	200-250 Hz Sweep
20616	04:34:00-04:34:10	600-700 Hz Sweep
20621	04:40:30-04:42:00	0-2 KHz Noise
20622	04:42:30-04:43:30	0-500 Hz Noise
20623	04:44:10-04:44:40	0-200 Hz Noise
20624	04:45:10-04:45:40	0-100 Hz Noise
20625	04:47:00-04:48:00	200-300 Hz Noise
20626	04:52:30-04:53:00	0-100 Hz Noise
20627	04:53:45-04:54:15	0-200 Hz Noise
20628	04:54:55-04:55:20	0-500 Hz Noise
20629	04:56:30-04:57:30	0-2 KHz Noise
20631	05:11:30-05:12:30	Vehicle Idling
20632	05:13:30-05:14:00	Vehicle Fast Idle
20633	05:15:30-05:16:00	Vehicle Exhaust
20634	05:16:40-05:17:10	Vehicle Zooming
20635	05:18:25-05:18:35	Engine Pass 5 MPH
20636	05:19:00-05:19:10	Engine Out Pass 5 MPH
20637	05:19:27-05:19:37	Engine Out Pass 10 MPH
20638	05:19:53-05:20:03	Engine On Pass 5 MPH
20639	05:20:25-05:20:35	Engine On Pass 10 MPH
20711	05:22:00-05:22:10	100-30 Hz Sweep
20712	05:22:40-05:22:50	30-50 Hz Sweep
20713	05:23:30-05:23:40	50-60 Hz Sweep
20714	05:24:20-05:24:30	60-70 Hz Sweep
20715	05:31:10-05:31:20	1000-100 Hz Sweep
20721	05:43:15-05:44:15	0-2 KHz Noise
20722	05:45:00-05:46:00	0-500 Hz Noise
20723	05:46:30-05:47:30	0-200 Hz Noise
20724	05:48:10-05:49:10	0-100 Hz Noise
20725	05:50:00-05:51:30	200-300 Hz Noise
20731	05:55:13-05:55:23	Engine Out Pass 5 MPH
20732	05:55:40-05:55:50	Engine Out Pass 10 MPH
20733	05:56:07-05:56:17	Engine On Pass 5 MPH
20734	05:56:29-05:56:39	Engine On Pass 10 MPH
20735	05:57:05-05:57:35	Engine Idling
20736	05:58:10-05:58:40	Engine Zooming
20737	05:59:15-05:59:45	Engine Exhaust
20738	06:00:35-06:01:05	Engine Exhaust Zooming
20801	06:02:00-06:03:00	Background
20811	06:05:38-06:05:48	30-50 Hz Sweep
20812	06:09:30-06:09:40	50-30 Hz Sweep
20813	06:10:30-06:10:40	30-100 Hz Sweep
20814	06:16:20-06:16:30	100-200 Hz Sweep
20815	06:17:53-06:18:03	200-300 Hz Sweep
20816	06:18:50-05:19:10	1000-300 Hz Sweep

SIGNAL NO.	TIME CODE	DESCRIPTION
20817	06:19:47-06:19:57	300-500 Hz Sweep
20818	06:21:38-06:21:48	500-700 Hz Sweep
20819	06:22:30-06:22:40	700-1000 Hz Sweep
20821	06:39:30-06:41:00	0-2 KHz Noise
20822	06:42:00-06:42:30	0-500 Hz Noise
20823	06:44:30-06:45:00	0-200 Hz Noise
20824	06:46:30-06:47:00	0-100 Hz Noise
20825	06:49:00-06:49:30	200-300 Hz Noise
20831	06:51:45-06:52:15	Engine Idle
20832	06:52:30-06:53:00	Engine Zooming
20833	06:53:50-06:54:10	Engine Exhaust Idle
20834	06:54:20-06:54:40	Engine Exhaust Zooming
20835	06:58:14-06:58:24	Engine Out Pass
20836	06:59:30-06:59:46	Engine On Pass
20837	07:01:00-07:02:00	Engine On Pass

Tape 3

SIGNAL NO.	TIME CODE	DESCRIPTION
30901	17:46:00-17:47:00	Background
30911	17:48:38-17:48:48	30-40 Hz Sweep
30912	17:51:50-17:52:00	50-70 Hz Sweep
30913	17:55:30-17:55:40	90-100 Hz Sweep
30914	17:59:00-17:59:10	100-150 Hz Sweep
30915	18:01:52-18:02:02	200-300 Hz Sweep
30916	18:06:20-18:06:30	1000-400 Hz Sweep
30917	18:08:50-18:09:00	400-500 Hz Sweep
30918	18:10:30-18:10:40	700-1000 Hz Sweep
30921	18:16:30-18:18:00	0-2 KHz Noise
30922	18:20:45-18:21:30	0-500 Hz Noise
30923	18:22:00-18:22:30	0-200 Hz Noise
30924	18:28:25-18:28:55	200-300 Hz Noise
30931	18:32:25-18:32:35	Engine Idle
30932	18:33:40-18:33:50	Engine Zooming
30933	18:34:20-18:34:30	Engine Fast Idle
30934	18:35:50-18:36:00	Engine Exhaust Idle
30935	18:37:20-18:37:30	Engine Exhaust Zooming
30926	18:39:14-18:39:24	Engine On Pass 5 MPH
30937	18:40:59-18:41:09	Engine On Pass 5 MPH
31001	18:43:30-18:44:30	Background
31011	18:46:55-18:47:05	30-50 Hz Sweep
31012	18:49:40-18:49:50	50-70 Hz Sweep
31013	18:51:36-18:51:46	80-50 Hz Sweep
31014	18:53:30-18:53:40	90-100 Hz Sweep
31015	18:56:25 18:56:35	200-300 Hz Sweep
31002	19:01:10-19:02:10	Background
31021	19:07:10-19:07:40	0-2 KHz Noise
31022	19:09:00-19:09:30	0-500 Hz Noise

SIGNAL NO.	TIME CODE	DESCRIPTION
31023	19:11:00-19:11:30	0-200 Hz Noise
31024	19:26:35-19:27:05	200-300 Hz Noise
31111	20:22:00-20:22:10	30-40 Hz Sweep
31112	20:22:50-20:23:00	40-50 Hz Sweep
31113	20:23:35-20:23:45	50-70 Hz Sweep
31114	20:26:45-20:26:45	90-100 Hz Sweep
31115	20:28:48-20:28:58	400-200 Hz Sweep
31116	20:30:47-20:30:57	400-500 Hz Sweep
31117	20:31:40-20:31:50	700-800 Hz Sweep
31121	20:35:35-20:36:15	0-2 KHz Noise
31122	20:37:50-20:38:20	0-500 Hz Noise
31123	20:38:55-20:39:25	0-200 Hz Noise
31124	20:40:00-20:40:30	0-100 Hz Noise
31131	20:42:30-20:42:40	Engine Idle
31132	20:42:55-20:43:05	Engine Zooming
31133	20:44:00-20:44:10	Engine Exhaust Idle
31134	20:44:25-20:44:35	Engine Exhaust Zooming
31135	20:45:22-20:45:32	Engine Out Pass 5 MPH
31136	20:46:07-20:46:17	Engine Out Pass 10 MPH
31137	20:47:03-20:47:13	Engine On Pass 5 MPH
31138	20:47:53-20:48:03	Engine On Pass 10 MPH
31221	20:48:40-20:49:40	0-2 KHz Noise
31222	20:50:30-20:51:30	0-1 KHz Noise
31223	20:52:20-20:52:50	0-500 Hz Noise
31224	20:53:10-20:53:40	0-200 Hz Noise
31225	20:54:05-20:54:35	0-100 Hz Noise
31231	20:55:00-20:55:10	Engine Idle
31232	20:55:35-20:55:45	Engine Zooming
31233	20:56:02-20:56:12	Engine Out Pass
31234	20:56:40-20:56:50	Engine On Pass

(The reverse of this page is blank)

INITIAL DISTRIBUTION

Hq USAF/RDQRM	2
Hq USAF/SAMI	1
Hq USAF/XOXFM	1
AFIS/INTA	1
AFSC/DLCA	1
AFSC/IGFG	1
AFSC/SDZA	1
AFAL/DHO	1
AFWAL/TECH LIB/FL2802	1
ASD/ENFEA	1
FTD/PDXA-2	1
AFML/LTM	1
AFWL/NSC	1
AFWL/NSE	1
AFWL/SUL	1
AUL (AU/LSE-70-239)	2
DDC	2
OGDEN ALC/MMWM	2
Picatinny Arsenal/SARPA-TS-S#59	1
Army Mat Sys Anal Agcy/DRXSY-J	1
Army Mat Sys Anal Agcy/DRXSY-A	1
Redstone Sci Info Ctr/Ch, Doc Sec	2
USAE Waterways Exp Stn/WESFE	1
NRL/Code 2627	1
NavAir Sys Comd/Tech Lib/AIR-954	1
NavSurWpnCen/Tech Lib & Info Svs Br	2
NavOrdStn/Tech Lib	1
NavAirTestCen/CT-176 TID/Tech Pubs	2
USNWC (Code 533)	1
Sandia Lab/Tech Lib Div 3141	1
The Rand Corp/Libr-D	1
TACTEC, Battelle Col Lab	1
TAWC/TRADOCLO	1
AFATL:	
DL	1
DLOSL	9
DLY	1
DLJ	1
DLJC	1
DLJF	1
DLJK	1
DLJM	1

(The reverse of this page is blank.)